Dissertation

Pathophysiological Mechanism of Endocardial Fibroelastosis Development in Hypoplastic Left Heart Syndrome

submitted by

Dr.med.univ.

Viktoria Heide-Marie WEIXLER

for the Academic Degree of

Doctor of Medical Science

(Dr.scient.med.)

at the

Medical University of Graz

Department of Cardiac Surgery

In cooperation with

Boston Children`s Hospital, Harvard Medical School

under the supervision of

Prof. Dr. Ameli YATES

Priv.-Doz. Dr. Ingeborg FRIEHS

Prof. Dr. Martin KÖSTENBERGER

2020

“The strongest hearts have the most scars”
(Jeff Hood)

This thesis is dedicated to all the children born with Hypoplastic Left Heart syndrome and their parents who never stop fighting.

Table of Contents

Statutory Declaration

I hereby declare that I have developed and written the enclosed thesis completely by myself, and have not used sources or means without declaration in the text. Furthermore I have acknowledged by name all those individuals and organizations that have contributed to this research. Any thoughts from others or literal quotations are clearly marked. This thesis was not used in the same or in a similar version to achieve an academic grade or is being published elsewhere. Throughout the thesis and in all related publications I followed the “Standards of Good Scientific Practice and Ombuds Committee at the Medical University of Graz”.

Graz, 08.03.2020 Dr. med. univ. Viktoria Heide-Marie Weixler

Disclosures

Part of this thesis has been published in the following articles:

***Weixler V**, Marx G, Hammer P, Emani S, del Nido P and Friehs I: Flow disturbances and the development of endocardial fibroelastosis. Journal of Thoracic and Cardiovascular Surgery. 2019*

***Weixler V**, Hammer P, Marx G, Emani S, del Nido P and Friehs I: Flow disturbances and the progression of endocardial fibroelastosis – a case report. Cardiovascular Pathology. 2019.*

Parts of the results have been presented at the 51st Annual Meeting German Society for Pediatric Cardiology in Wiesbaden (Germany) in January 2019:

*Vorisek C, **Weixler V**, Axt-Fliedner R, del Nido P, Friehs I: Possible Inhibitors of Endothelial-to-Mesenchymal Transition Targeting Endocardial Fibroelastosis. Thorac cardiovasc Surg 2019; 67 (S 02)*

All contributing authors (listed in alphabetical order) have been asked for permission and explicitly agreed to the use of their data in this thesis:

Prof. Dr.med. Axt-Fliedner Roland
Division of Prenatal Medicine, University of Gießen and Marburg, Germany

Del Nido Pedro, MD
Department of Cardiac Surgery, Boston Children's Hospital, Harvard Medical School, USA

Emani Sitaram, MD
Department of Cardiac Surgery, Boston Children's Hospital, Harvard Medical School, USA

PD Dr. Friehs Ingeborg
Department of Cardiac Surgery, Boston Children's Hospital, Harvard Medical School, USA

Hammer Peter, PhD
Department of Cardiac Surgery, Boston Children's Hospital, Harvard Medical School, USA

Marx Gerald, MD
Department of Cardiology, Boston Children's Hospital, Harvard Medical School, USA

Dr. med. Vorisek, Carina
Department of Cardiac Surgery, Boston Children's Hospital, Harvard Medical School, USA

All animals received humane care from the Animal Resources of Boston Children's Hospital and all protocols were reviewed and approved by the Institutional Animal Care and Use Committee (IACUC) at Boston Children's Hospital, affiliated with Harvard Medical School.

All experiments performed using human tissue were performed with approval of the institutional review board of Boston Children's Hospital, affiliated with Harvard Medical School.

Due to the originality and novelty of this work, parts of the 'results' and 'discussion' section of this thesis were taken from the two following publications, in which I am listed as first author:

Weixler V*, Marx G, Hammer P, Emani S, del Nido P and Friehs I: Flow disturbances and the development of endocardial fibroelastosis. Journal of Thoracic and Cardiovascular Surgery. 2019*

Weixler V*, Hammer P, Marx G, Emani S, del Nido P and Friehs I: Flow disturbances and the progression of endocardial fibroelastosis – a case report. Cardiovascular Pathology. 2019.*

I hereby confirm that these publications belong to my own intellectual property and that I have furthermore asked for copyright permission at the individual journals. I cited these two publications to my best knowledge and have no further conflict of interest.

Acknowledgements

It is with mixed emotions that I write this acknowledgement section of my thesis, as it signifies that I truly have come to the end of this incredibly challenging, yet rewarding journey. As such, I would like to take this opportunity to acknowledge those whose valuable guidance and support have made it possible for me to complete this work.

First of all I would like to express my special thanks to my external supervisor Priv.-Doz. Dr.med. Ingeborg Friehs, who not only welcomed me in her lab at Boston Children's Hospital despite very little research experience and taught me the fundamentals of research but also completely changed my way of thinking. Although it was difficult to fully grasp her teaching methods at the outset, it turned out to be the most instructive experience I could ever have. Upon reflection, she will always be one of my greatest teachers in medicine and life.

Secondly, I would like to thank my institutional supervisor and close friend Univ.-Prof. Dr.med. Ameli Yates for giving me the opportunity to conduct my doctoral thesis at the Department of Cardiac Surgery at Medical University Graz, Austria. From the very first day, I stepped into her OR, still as a medical student in my practical year, she always believed in me and encouraged me to excel and pursue my dreams. It was her faith, trust and guidance that led to her becoming the first mentor to inspire me to pursue cardiac surgery. As we became close friends throughout the years, my respect for this amazing female cardiac surgeon only grew. I watched her demonstrate that it is in fact possible to have it all- career and family!

Thirdly, I would like to thank my third supervisor and pediatric cardiologist Univ.-Prof. Dr. Martin Köstenberger, and pediatric cardiac surgeons Univ.-Prof. Dr.med. Igor Knez and Dr. Elisabeth Beran, for introducing me to pediatric cardiac surgery, and inspiring me to pursue this field of medicine.

In addition, I would like to thank the numerous pediatric cardiac surgeons whom I had the pleasure of working with throughout my residency and research years, in particular for helping me to better understand the complex congenital heart defect of Hypoplastic Left Heart Syndrome. Whilst this list is certainly not exhaustive, I would like to make special mention of Dr. Pedro del Nido, Dr. Sitaram Emani, Prof. Dr. med. Joachim Photiadis, Dr. Mi-Young Cho, Dr. Peter Murin and Prof. Dr. med. Gerardus Bennink for their particular assistance during this time.

Cordial thanks go to all my colleagues and friends; I met during these 2 years of living in Boston, who have been an amazing support throughout a very strenuous but incredibly memorable time of my life. Just to mention a few: Margherita, Emeline, Marta, Carina, Alvise, George, Steven, Alberto, Ali and many more.

Lastly, I would like to thank my devoted parents Josef and Walpurga, who have supported my every pursuit and have encouraged me to continue learning over the years. They have been exceptional role models, and I hope to continue making them proud for years to come.

This thesis was conducted through the Doctoral School Translational Molecular and Cellular Biosciences at Medical University of Graz.

List of figures

List of tables

Abbreviations and Definitions

(R)-SMADs
Regulatory SMADs 25
AA
Aortic atresia 16
ALK
Actin receptor-like kinases 25
AMH
Anti-müllerian-hormone 24
AS
Aortic stenosis 16
AV
Aortic valve 23
BMP
Bone morphogenic protein 24
DMSO
Dimethyl sulfoxide 33
EC
Endothelial cells 30
ECM
Extracellular matrix 50
EFE
Endocardial Fibroelastosis 17
EMT
Epithelial-to-mesenchymal-transition ... 23
EndMT
Endocardial-to-mesenchymal-transition 23
EZ
Endothelzellen 12
FSP
Fibroblast specific protein 23
GDF
Growth and differentiation factor 24
HCAEC
Human coronary endothelial cells 30
HLHS
Hypoplastic Left Heart Syndrome 16
HTX
Heart transplantation 21
LVOT
Left ventricle outflow tract 16
MA
Mitral atresia 16
MMPs
Matrix metalloproteinases 50
MS
Mitral stenosis 16
MV
Mitral valve 18
OCT
Optimal cutting temperature 48
PA
Pulmonary atresia 18
PAB
Pulmonary artery banding 19
PBS
Phosphate buffered salin 31
PDA
Patent Ductus arteriosus Botalli 16
PFA
Paraformaldehyde 35
PGE
E-type prostaglandin 16
REEC
Rat endocardial endothelial cells 30
RV
Right ventricle 48
TGF-β
transforming growth factor ß 23
vWf
von-Willebrand-factor 23
α-SMA
α –smooth muscle cell actin 23

Zusammenfassung

Hintergrund: Endotheliale-mesenchymale Transition (EndMT) spielt eine wesentliche Rolle bei der Entstehung der kardialen Fibrose einschließlich der Endokardfibroelastose (EFE), die mit kongenitalen Herzerkrankungen wie dem hypoplastischen Linksherzsyndrom (HLHS) assoziiert ist. Die Stimuli für EndMT, die zur Entstehung von EFE führen sind noch unbekannt, aber wir vermuten, dass mechanische Kräfte und junges Alter mit der Entstehung dieser besonderen Form von Fibrose vergesellschaftet sind. Die Ziele dieser Studie waren es diese Stimuli und regulatorische Signalwege, die zur Entstehung von EFE führen, zu identifizieren.

Material und Methoden: Endothelzellen (EZ) in einer *in vitro* Zellkultur wurden 8h lang 10% uniaxialer Dehnung oder direkter EndMT-Stimulation durch Zugabe von TGF-ß in das Medium, zugeführt. Die Hemmung des TGF-ß Signalwegs wurde durch lokale Applikation von BMP7, dem direkten TGF-ß-Inhibitor SB431542 und Losartan durchgeführt. Unreife und reife isolierte und perfundierte Rattenherzen (n=7/Gruppe) wurden für 3h mit einem Gewicht, befestigt am Apex, gedehnt. Es wurden die gleichen Gruppen wie in den in vitro Zellkulturexperimenten verwendet. Zusätzlich wurde EFE Gewebe, welches von Patienten mit Hypoplastischen Linksherzsyndrom (HLHS) aus dem linken Ventrikel reseziert wurde und zusätzlich makroskopisch ‚EFE-ähnliches' Gewebe von 6 nicht-HLHS Patienten mit Flussturbulenzen im linken Ventrikel analysiert. Der Gehalt an Collagen/Elastin, Kapillar-/Zelldichte sowie das Vorhandensein von aktiven EndMT wurde durch immunohistochemische Färbungen bestimmt. Die Umwandlung des Gewebes vom Untergang der elastischen-/collagenreichen Fasern durch Matrixmetalloproteinasen wurde durch *in situ* Zymographie bestimmt.

Ergebnisse: Dehnung induzierte EndMT in isolierten EZ in Kultur wurde durch signifikant mehr CD-31/alpha-SMA doppel-gefärbte Endothelzellen in der in vitro Zellkultur (46±13% der totalen Zellzahl) bestimmt und in den ex vivo isolierten Herzen (15.9±2% der totalen Zellzahl) bestätigt

verglichen zu Kontrollen (Zellen: 7±2%; Herzen: 3.1±0.1; $p<0.05$). Jedoch konnte EndMT nur in den unreifen Herzen induziert werden. Durch Hemmung des TGF-ß Signalwegs sank die Zahl an doppel-gefärbten Zellen signifikant auch nach Dehnung, verglichen zu den Kontrollen (Zellen/Herzen: Kontrolle: 7±2/3.1±0.1%, Dehnung: 46±13/15±2%, BMP7: 7±2/2.9±0.1%, 5.2±1.3%, Losartan (nur Herzen) 0.89±0.1%; $p<0.001$). ‚EFE-ähnliches' Gewebe von nicht-HLHS Patienten zeigte die gleichen Charakteristika als EFE Gewebe von HLHS Patienten. Aktive EndMT wurde in allen 24 HLHS Patienten und in den 6 nicht-HLHS Patienten gefunden. In den nicht-HLHS Patieten wurden Herzklappenerkrankungen, die hauptsächlich zu einem Jet über einer verengten Mitralklappe führten, gefunden. In situ Zymographie zeigte eine Balance zwischen Degratierung von Elastin/Collagen und Elastase/Gellatinase-Aktivitiät.

Schlussfolgerung: EndMT wurde in den *in vitro* und *ex vivo* Experimenten durch mechanische Dehnung am Endokard induziert, allerdings nur in den unreifen Herzen. Durch den Einsatz verschiedener Inhibitoren wie BMP-7 und Losartan, wurde der TGF-ß Signalweg als Hauptstimulator für die Entstehung von EndMT identifiziert. Mechanische Kräfte wie Flussturbulenzen und Dehnung setzen Endothelzellen verschiedenen Scherkräften aus, die die Trigger für die Entstehung von EndMT sind. In der menschlichen EFE Pathologie, führt eine verlängerte Exposition von Endokardzellen gegenüber wechselnden mechanischen Kräften zu einem Wiederauftreten von EFE in einer zunehmend infiltrativen Form in das darunterliegende Myokard. Diese Alterationen sind nicht nur auf den kongenitale Herzfehler des HLHS begrenzt sondern treten in Zusammenhang mit schweren Herzklappenerkrankungen mit Flussturbulenzen auf.

Abstract

Background: Endothelial-to-mesenchymal-transition (EndMT) plays a major role in cardiac fibrosis, including endocardial fibrosis (EFE), which is associated with congenital heart defects such as hypoplastic left heart syndrome (HLHS). The stimuli for EndMT leading to EFE formation are still unknown but we speculate that mechanical forces and young age are associated with the development of this unique form of fibrosis. The aims of the study were to identify stimuli and regulator pathways leading to the development of EFE.

Material and Methods: Endothelial cells (EC) in culture were exposed to 8hrs of 10% uniaxial stretch or direct stimulation of EndMT through addition of TGF-b to the media. Inhibition of the TGF-β pathway was performed by local application of: BMP7, a TGF-ß inhibitor SB431542 or Losartan. Immature and mature isolated perfused rat hearts (n=7/group) were exposed to 3h stretch through a weight attached to the apex of the LV. The same groups as in the isolated cell culture experiments were tested. Additionally, EFE tissue resected from the LV of 24 HLHS patients and macroscopically 'EFE-like' tissue of 6 non-HLHS patients with known flow disturbances in the LV outflow tract was analyzed. Amount of collagen/elastin, vascularity/cellularity and presence of active EndMT was determined by immunohistochemical staining. Tissue remodeling through degradation of elastic fibers/collagen by matrix metalloproteinases was determined by in situ zymography.

Results: Stretch induced EndMT in isolated ECs in culture was determined by significantly more CD-31/alpha-SMA double-stained endothelial cells (46±13% of total cell count), and confirmed in whole hearts (15.9±2% of total cell count) compared to controls (cells: 7±2%; heart: 3.1±0.1;

$p<0.05$). However, only immature hearts showed endocardial EndMT. Inhibition of the TGF-ß pathway significantly decreased the number of double-stained cells following stretch, comparable to controls (cells/heart: control: 7±2/3.1±0.1%, stretch: 46±13/15±2%, BMP7: 7±2/2.9±0.1%, 5.2±1.3%, Losartan (heart only): 0.89±0.1%; $p<0.001$).

"EFE-like" tissue obtained from non-HLHS patients, showed the same characteristics as EFE tissue from HLHS patients. Active EndMT was found in all 24 HLHS samples and all 6 non-HLHS patients. In the "non-HLHS" patient group with valvar disease, predominantly a jet across a stenotic mitral valve was present. In situ zymography displayed a balance between degradation of elastin/collagen and elastase/gelatinase activity.

Conclusion: EndMT was induced in in vitro and ex vivo experiments by mechanical strain on the endocardium, however, only in immature hearts. By use of specific inhibitors such as BMP-7 and Losartan, the TGF-ß pathway was identified as the main stimulator for EndMT development. Mechanical forces such as flow disturbances and stretch exposing endocardial endothelial cells to altered mechanical force are triggers for induction of EndMT. In human EFE pathology, prolonged exposure of endocardial endothelial cells to altered mechanical forces leads to reoccurrence of EFE displaying with a more infiltrative growth pattern into the underlying myocardium. These alterations are not limited to HLHS but are associated with severe congenital valve diseases with flow turbulences.

1. Introduction

1.1. Hypoplastic Left Heart Syndrome (HLHS)

HLHS was first described by Canton (1) in 1850 as an underdevelopment of the left sided structures of the heart. Even today it is still the most lethal congenital heart disease, accounting for 25-40% of all neonatal cardiac deaths (2). It is rather rare occurring in about 1/4000 livebirths in the United States which accounts for 2-3% of all congenital heart diseases (3).

HLHS is characterized by hypoplasia of the left sided structures of the heart, covering a wide spectrum with various severity from a simple aortic stenosis (AS) due to a bicuspid valve to a complex congenital malformation with a rudimentary left ventricle (LV) and/or outflow tract (LVOT) and an interrupted aortic arch. There are different subtypes due to different degrees of hypoplasia of the LV and the ascending aorta, AS, aortic atresia (AA), mitral stenosis (MS) or mitral atresia (MA) (1). In case of an underdeveloped LV at birth, the inability to support a systemic circulation makes this a lethal disease if left untreated. As long as there is a right-to-left connection through a patent ductus arteriosus (PDA) the right ventricle can support the systemic circulation immediately after birth. As the ductus naturally closes shortly after birth, though, it leads to cyanosis and eventually to death (4). E-type prostaglandins (PGE) are used to keep the ductus open and therefore stabilize the patient until surgery (5). Furthermore, more recent hybrid procedures have been introduced to stabilize the newborn (6).

1.2.Diagnosis and Prenatal Management

Fetal echocardiography is constantly improving and allows for the visualization of an abnormal four-chamber view because of a stenotic aortic valve or a small LV in about two-thirds of all cases of HLHS between 18 and 24 weeks of gestation (7,8). Improved prenatal diagnosis has two major roles in the management of HLHS. First of all, with an early diagnosis, postnatal management can be planned ahead of delivery, prostaglandin E1 can be provided immediately after birth to keep the PDA open, and specialized centers can be contacted to get involved in the management of the patient. Secondly, in specialized centers fetal interventions such as aortic valvuloplasty are available for a selected patient cohort who were diagnosed with critical AS but a still normally sized LV in the second trimester (9).

The first fetal aortic balloon valvuloplasty was performed in 1989 using an 18- to 19-gauge needle to gain percutaneous access to the uterus and the fetus; in 2000, this procedure was first used in HLHS. By passing a balloon across the aortic valve and dilating the stenotic valve, LV afterload decreases, reconstituting forward flow through the left heart preventing severe left heart dysfunction. After successful dilatation of the aortic valve, the LV and its structures maintain growth and LV hemodynamics are improving (10,11). Fetal aortic balloon valvuloplasty can lead to a biventricular circulation in 30% of the patients after birth. An additional 8% of patients where the LV cannot support the systemic circulation, undergo a unique surgical management which was introduced by Boston Children's Hospital. The goal of this combined prenatal and postnatal management is to rehabilitate the left ventricle for future biventricular circulation (9,12).

Whether fetal balloon valvuloplasty is successful and biventricular circulation can be accomplished, depends primarily on the size of the LV. A thick, whitish, echo-bright fibroelastic tissue layer covering the inner surface of LV cavity (endocardium) could be identified as one of the determining factors for pre- and post-natal adaptation of the LV. This tissue is known as 'Endocardial Fibroelastosis' (EFE). It could be shown that the extend of EFE at the time of intervention is correlated with growth restriction of the LV (13,14). As a next logical step, Boston Children's Hospital combined prenatal intervention with postnatal surgical removal of EFE under the assumption that EFE removal would allow for catch-up growth postnatally (15).

1.2.1 Grading Degree of EFE through Fetal Echocardiography

To predict postnatal outcome after *in utero* aortic balloon valvuloplasty, a grading system for pre-interventional echocardiographic images was established. For this study, pre-intervention fetal echocardiograms from 74 patients undergoing *in utero* aortic valvuloplasty were analyzed by two different echocardiographers who classified EFE severity through 4 different grades (0-3) depending on the echogenicity (0-3) **(See Figure 1).**

Grading system of EFE severity:

Grade 0 = No EFE

Grade 1 = mild EFE (scattered echogenic spots within the LV)

Grade 2 = moderate EFE (non-contiguous echogenic patches throughout the LV)

Grade 3 = severe EFE (contiguous echogenic lining of the LV)

EFE on the ventricular septum: more prominent than rest of LV (0=no, 1=EFE present but not more prominent than elsewhere, 2= EFE present and more prominent on septum than elsewhere)

Echogenic papillary muscles (1=yes; 0=no)

Presence of an immobile, echogenic **strand running between mitral valve (MV) or tension apparatus and the LV outflow tract** (1=yes, 0=no) (14).

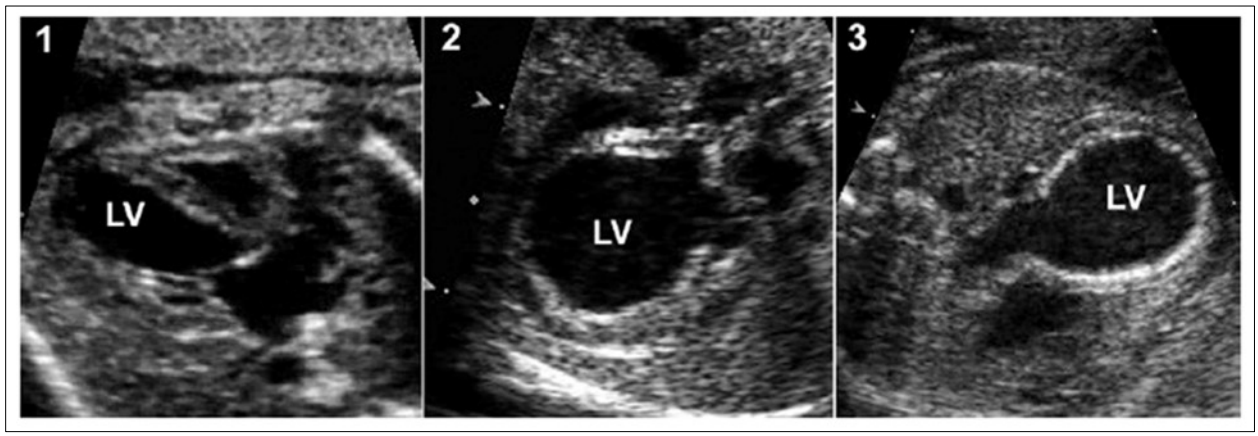

Figure 1: Grading System of EFE severity, reproduced from McElhinney et al. (2010) with permission of Elsevier. Grade 1 (mild EFE), grade 2 (moderate EFE) and grade 3 (severe EFE).

1.3. Postnatal Management of HLHS

1.3.1. Norwood Procedure

Indication for treatment of HLHS exists by the time of diagnosis. As described above, to maintain a communication between the right and left circulation, PGE1 to keep the PDA open is administered immediately postnatally to prevent low-output syndrome and accompanied metabolic acidosis. After stabilization and afterload reduction, the three-stage Norwood procedure is performed. Bill Norwood and colleagues introduced this three-stage palliative concept at Boston Children's Hospital first in the 1980s (16,17) **(See Figure 2).**

The Stage 1 Norwood procedure, which is normally performed on cardiopulmonary bypass in circulatory arrest and 18°C hypothermia, the ductus arteriosus Botalli is ligated and the pulmonary artery (PA) is transected. The proximal PA is connected to the repaired hypoplastic aortic arch with a homograft, while the distal PA is closed with pericardium. Thus, the right ventricle can

drain blood into the systemic circulation, whilst blood flow from the right ventricle to the lungs is disrupted. To provide pulmonary perfusion, the brachiocephalic trunk is connected to the right pulmonary artery through a modified Blalock-Taussig shunt. With this step, the right ventricle serves as the ventricle supporting the systemic circulation. In high-risk HLHS patients, such as patients with a restrictive atrial septum, preoperative hemodynamic instability, moderate to severe dysfunction of the dominant ventricle or obstructive pulmonary venous return, the postoperative survival-rate after Stage I Norwood is decreasing dramatically. In this selected patient cohort, a combination of pulmonary artery banding (PAB), maintenance of the ductus arteriosus Botalli by applying prostaglandin or stenting, and arterial septostomy, a so-called 'hybrid procedure', is performed as primary palliation, until staged Norwood procedure is possible. This procedure has been first described by Akintuerk and collogues in Giessen (Germany). Studies have shown that patients undergoing this primary palliation, have comparable mortality rates as patients undergoing staged Norwood procedure (6).

After about 4-6 months, Stage 2 of the Norwood procedure is performed to separate the systemic and pulmonary circulation. Therefore, the aortopulmonary connection is removed and the superior vena cava is transected and bidirectionally connected to the pulmonary artery by a Glenn anastomosis.

Stage 3 of Norwood procedure is performed 2-3 years later. It connects the inferior vena cava either through an intra-atrial tunnel to the pulmonary artery or with an extracardiac conduit to name the most common surgical connections (Fontan surgery) (18). Although outcome and survival rates after surgical repair are constantly improving, cumulative mortality following three surgical interventions is still high and survival at 5 years is around 65% and drops to 55% at 10 years (2,4). Due to decreased exercise tolerance over time, and the sequela observed as a consequence of the Fontan circulation such as thromboembolic events, arrhythmia, plastic bronchitis or protein-loss enteropathy, eventually cardiac transplantation is inevitable (19).

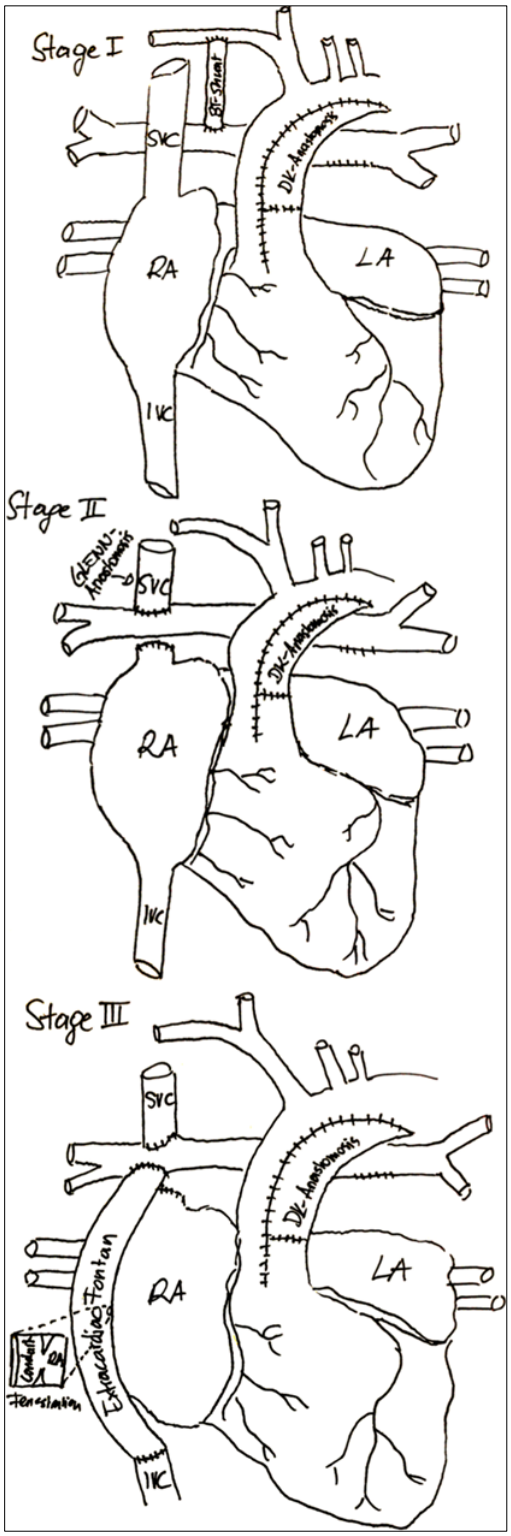

Figure 2: Stage 1, 2 and 3 of Norwood procedure (© V. WEIXLER)

1.3.2. Biventricular Conversion

Biventricular Conversion is desirable in all HLHS patients as a biventricular circulation is considered superior to an univentricular heart. Studies have shown that in borderline HLHS patients, low left ventricular end diastolic pressures (LVEDP<13mmHg) and LV end diastolic volumes of >22ml/min are predictors for a favorable outcome with a low mortality rate after biventricular conversion (20).

1.3.3. Cardiac Transplantation

Since the first successful heart transplantation (HTX) in humans by Christiaan Barnard in 1967, HTX has turned from an experimental stage to a therapeutic option in patients with end-stage heart failure (21). Due to the progress in modern cardiac surgery, up to 90% of patients with complex congenital heart defects survive adulthood nowadays and many of these patients require HTX at some point (22). However, HTX is not so much a therapeutic option but a final resource of treatment necessitating life-long medication and re-transplantation in the future. Furthermore, organ shortage does not allow for more than 100 heart transplants per year in infants and only a few specialist centers around the world offer this treatment option for neonates and infants (23,24). Even after transplantation, patients are facing challenges of antibody-mediated rejection and long-term morbidities such as renal failure. Due to these limitations, Norwood procedure became the gold standard and cardiac transplantation remains an option in a selected group of patients who are unsuitable for a staged-reconstruction (25).

1.4. Endocardial Fibroelastosis (EFE)

The term EFE was first described by Weinberg and Himelfarb in 1943. Pathological specimens assign EFE to about 1.6% of all newborns suffering from heart disease. It is characterized by a fibroelastic thickening of the endocardium predominantly affecting the left ventricle **(See Figure 3)**

Published reports distinguish between a primary form, which is not caused by structural abnormalities of the heart, and a secondary form, which is associated with several diseases including congenital heart diseases such as the HLHS, as described above. (1,26). It is also associated with various other extracardiac anomalies (28%) such as Turner Syndrome, trisomy 13,

18 or 21, respectively, diaphragmatic hernias, omphaloceles, lysosomal storage diseases (27) or immunologic diseases (28).

One of the current running hypothesis is that EFE restricts the growth of the LV. Removal of EFE in young infants has been shown to result in improvement of restriction, and catch-up growth of the left ventricle occurs which is in support of our hypothesis (15,29). This finding strongly supports the notion that EFE plays a major role in the progression and ultimately outcome on whether a one ventricular palliation or two ventricular correction can be accomplished for patients with HLHS.

Thus, from a therapeutic perspective, I took a closer look at the underlying molecular mechanism of EFE development, which still remains unclear.

Clinical observations indicate that EFE constitutes a de-novo subendocardial tissue layer encapsulating the myocardium, which at a young age, can be easily removed surgical without major myocardial contamination (29). With access to this tissue, this led to a series of experiments which followed the hypothesis that the origin of EFE is rather endocardial than myocardial. My research group previously identified that the main cell type in EFE tissue are cells double-staining for endothelial and mesenchymal markers at the same time which is indicative of endothelial-to-mesenchymal-transition (30,31). Thus, endocardial endothelial cells in areas of EFE formation change their phenotype and undergo transformation into fibroblasts which produce and deposit collagen and elastin.

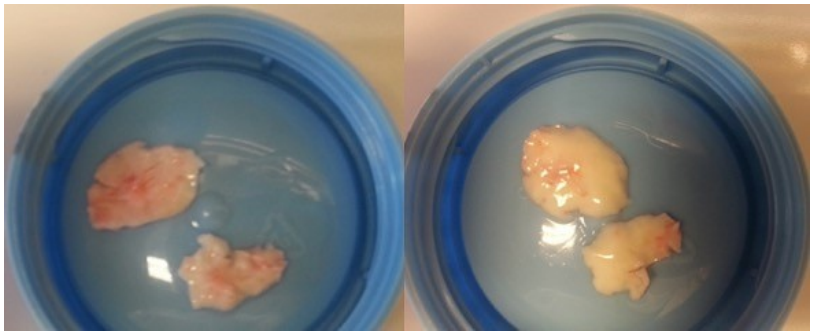

Figure 3: Macroscopic appearance of EFE as a thick whitish layer within left ventricle of individuals with HLHS, left picture: side facing towards the myocardium, right picture: side facing towards ventricular chamber (© V. WEIXLER)

1.5. Endothelial-to-Mesenchymal-Transition (EndMT) and Its Regulation

The process transforming endothelial cells to mesenchymal cells is termed endothelial-to-mesenchymal-transition (EndMT), which is a form of epithelial-mesenchymal transition (EMT). During embryologic development of valves and septa of the heart, EndMT is a necessary process forming valves out of the atrioventricular cushions (30).

Whereas being a useful process during the development of (AV) valves and the membranous interventricular septum, which both arise from embryogenic endothelial cells, EndMT also is described under pathologic conditions such as organ fibrosis (32), vascular diseases or cancer (33,34).

During the process of EndMT, endothelial cells organized as an inner cell layer of the vessel wall, disconnect and lose their cell-cell junctions, and migrate into the underlying tissue. At this point of transition, endothelial cells display endothelial as well as mesenchymal markers which over time change to become fibroblasts. Markers for mesenchymal tissue such as CD44, vimentin, fibroblast specific protein (FSP) 1, α-smooth muscle cell actin (α-SMA) and neural (N)-cadherin are upregulated, while endothelial markers such as CD31/Pecam-1 and vascular-endothelial (VE)-cadherin and von-Willebrand-factor (vWf) are downregulated (35,36). The current gold standard for identification of active EndMT is histological staining with endothelial and mesenchymal markers. Double-staining of cells is indicative of EndMT and Xingbo et al. demonstrated by using immunofluorescence staining in human EFE tissue samples obtained from HLHS patients that cells in human EFE tissue undergo this change from endothelial to mesenchymal cell by expressing both markers (31) **(See Figure 4).**

There are several triggers for EndMT described in the literature such as alterations in shear stress (37,38), ventricular mechanical stretch (39), hypoxia (40), inflammation (41), metabolic alterations such as high glucose levels, and tissue damage (42). The majority of these stimuli trigger the transforming growth factor ß (TGF-β) pathway activation which is one of the main signaling mechanisms responsible for the induction of EndMT.

Other known signaling pathways are Wnt/*β*-catenin (43), Notch (44) and various receptor tyrosine kinase pathways.

All these pathways culminate in the activation of transcription factors such as twist, SLUG or SNAIL, which then repress endothelial cell genes such as VE-cadherin and express mesenchymal cell genes which leads to phenotypical change of endothelial cells to mesenchymal cells (45).

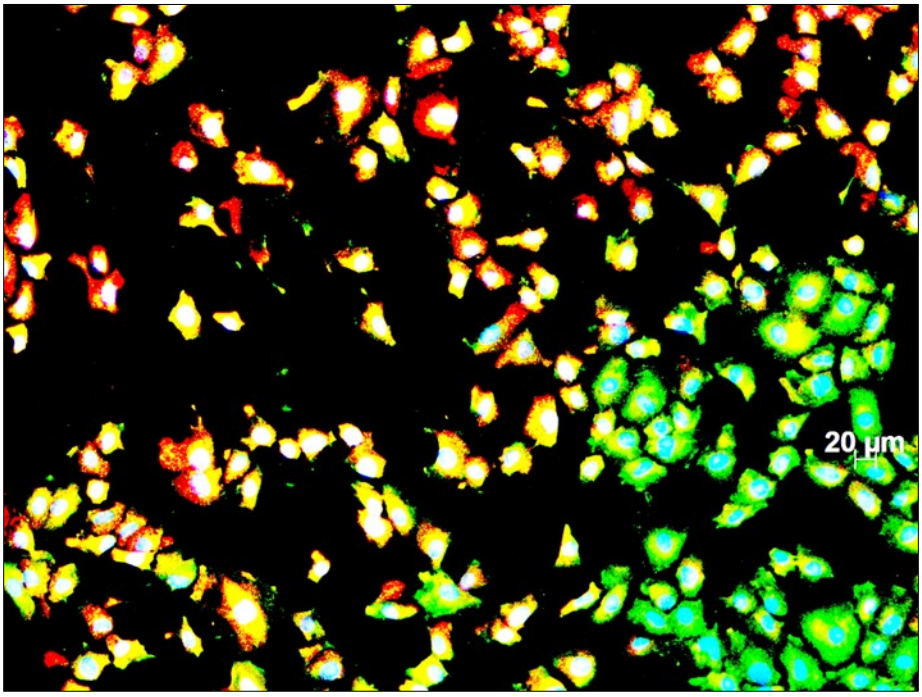

Figure 4: Endothelial cells (EC cells) undergoing EndMT, Green= endothelial marker (PECAM-1), Red= mesenchymal marker (alpha-SMA), Blue= DAPI (nuclei), on the right side nicely shaped endothelial cells, only stained with the green marker, on the left side, cells moving away from the cell-cell-contacts and are stained for both markers (red and green) (© V. WEIXLER)

1.6. TGF-β Signalling Pathway

As already mentioned, the TGF-ß-superfamily plays an important role in the regulation of EndMT. There are different members of the TGF-β superfamily (BMPs), Anti-müllerian hormone (AMH), growth and differentiation factors (GDFs), Activin, and TGF-β) that have multiple effects by binding specific transmembrane receptors. There are two distinct branches of the TGF-ß-superfamily, on the one hand the TGF-β-branch (TGF-β, nodal, activing) and on the other hand the BMP-branch (BMPs, growth and differentiation factors) which are maintained in balance (46). While TGF-ß and BMP2 and 4 (47,48) are inducing the process of EndMT, BMP7 was shown to be a negative regulator of EndMT (31).

First, signaling is initiated by binding of different TGF-ß-superfamily members to a receptor type II, a serine/threonine kinase receptor, which then phosphorylates a receptor type I. There are 7 different type I receptors (actin receptor-like kinases, ALK1 - ALK7) and 5 different type II receptors (activing receptor type IIA (ActRII-A), activin receptor type IIB (ActRII-B), bone morphogenetic protein type II receptor (BMPR-II), TGF-β type II receptor (TGFβR-II) and AMHtype II receptor (AMHR-II)). Different members of the TGF-ß-superfamily can bind to different types of receptors.(49)

TGF-β binds specifically to the receptors ALK2, ALK4, ALK5, ALK7 and TGFβRII, whereas BMP binds to the receptors ALK 1, ALK2, ALK3, ALK6, BMPR-II, ActRII-A and ActRII-B (49). After the ligands bind to the specific receptors on the cell surface, specific cytosolic intermediary factors called receptor-regulated (R)-SMAD proteins are phosphorylated and activated. (R)-SMADs then form complexes with the common mediator (co)- SMAD (SMAD4) and translocate into the nucleus, where they regulate the transcription of target genes through activation of specific transcription factors. Inhibitory (I)-SMADs at the same time prevent the activation of (R)-SMADs and eventually the downstream activation of TGF-ß signaling intermediaries (50).

SMAD 1/5/8 are activated by ALK3 and 6 and transduce BMP7 binding, whereas SMAD 2 and 3 are activated by ALK 2 and ALK5 and transduce TGF-β binding.

The binding of TGF-β1 to ALK2 and ALK5 leads to a phosphorylation of SMAD 2 and SMAD3, which results in the decrease of the VE-Cadherin and CD31, and an increase of alphaSMA and vimentin indicative of active EndMT.

In contrast, BMP7 binds to ALK3 and ALK6 receptor, which phosphorylates SMAD1/5/8 results in upregulation of Snail leading to increased transcription of VE-cadherin and CD31 preserving the endothelial phenotype and inducing angiogenesis (31,51).

Additionally, TGF-β has two signaling co-receptors called endoglin and betaglycan (TGF-β receptor III), which can cause either an enhancing or a conferring of TGF-β signaling depending on which ligand is binding, BMP or TGF-β (52,53).

In addition to SMAD-regulated signaling pathways, there is also a SMAD-independent pathway including several MAP kinase pathways, Rho-like GTPase signaling pathways and PI3K/AKT pathways (50) **(See Figure 5).**

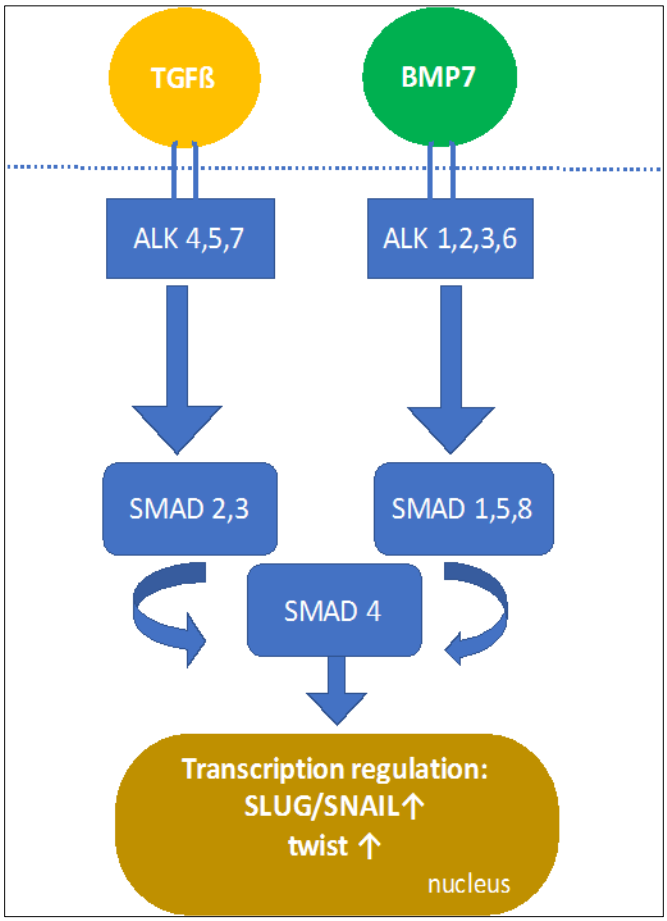

Figure 5: TGF-β1 and BMP7 signaling pathways in endothelial cells, activation of the TGF-β1 signaling pathway inhibits the VE-Cadherin promotor and therefore induces migration and proliferation of cells through phenotypical change of endothelial cell to fibroblasts, whereas activation of the BMP7-pathway preserves VE-Cadherin and the endothelial cell phenotype. (© V. WEIXLER)

1.7. EndMT in HLHS

As described above, the presence of EFE is associated with several cardiac and non-cardiac diseases; in our specific case, we are focusing on EFE in the LV of patients with HLHS.

It is unknown what triggers EFE formation but there are several potential candidates.

Clinical observation and animal studies indicate that EFE development is associated with mechanical alterations affecting flow or stretch. As my research group has shown, aortic regurgitation leading to intraventricular flow alterations and ventricular distention in a heterotopically transplanted neonatal rat heart induced EndMT in the LV of the transplanted heart

within 1 week. Transplanted adult hearts, however, did not develop EndMT, which suggests that immaturity of the heart is an additional influencing factor playing a role in the EndMT development (39).

Clinical observation indicates that EFE development depends on the developmental stage of a fetus or a young infant, and progression and reoccurrence of EFE growth has been shown to be self-limiting as the child grows older. At Boston Children's Hospital, so far the oldest child where EFE was diagnosed and resected was 11 years of age. Another trigger, which is hypothesized for EFE in HLHS, is the lack of flow in the LV. In an in-vivo rat heart model, Friehs et al. could show that a heterotopically transplanted unloaded neonatal heart develops EFE, whereas a loaded heart on the other side did not develop EFE (54).

1.8. Concepts of Inhibition of EndMT

As described above, the presence of EFE tissue in many diseases such as HLHS can be a limiting factor in terms of the outcome. Elucidating the underlying mechanism for EFE formation as EndMT now allows for inhibition of EndMT and thus, inhibition of the development and progression of EFE. In order to study potential treatment options, I introduced different *in vitro* models of isolated cell culture and an *ex vivo* whole heart preparation.

First, a cell culture model was used to simulate flow alterations or strain and to study exposure of endothelial cells to these different conditions. I used this model as proof-of-concept to show that endothelial cells undergo EndMT when exposed to different flow and strain conditions. Furthermore, the study goal was to determine whether EndMT in these circumstances was regulated by TGF-β.

Secondly, an *ex vivo* whole heart preparation was used to validate the isolated endothelial cell culture experiments and to show that the findings are reproducible in a whole heart preparation as well. TGF-β stimulation was evaluated by applying different TGF-β inhibitors.

In vivo animal studies using the principle of the heterotopic heart transplantation in neonatal rats had shown that EndMT can be inhibited by applying BMP7, which directly blocks the TGF-ß-induced upregulation of VE-cadherin (31).

Another way of EndMT inhibition is to block the binding of TGF-ß to the receptors such as the ALK5 kinase inhibitor SB-431542, which was shown in an *in vitro* cell culture studies to upregulate claudin-5, a component of the endothelial tight junction, which is responsible for cell-

cell contacts (55). Losartan on the other hand is a clinically-used angiotensin receptor inhibitor which additionally blocks the TGF-ß pathway indirectly (56) (**See Figure 6**).

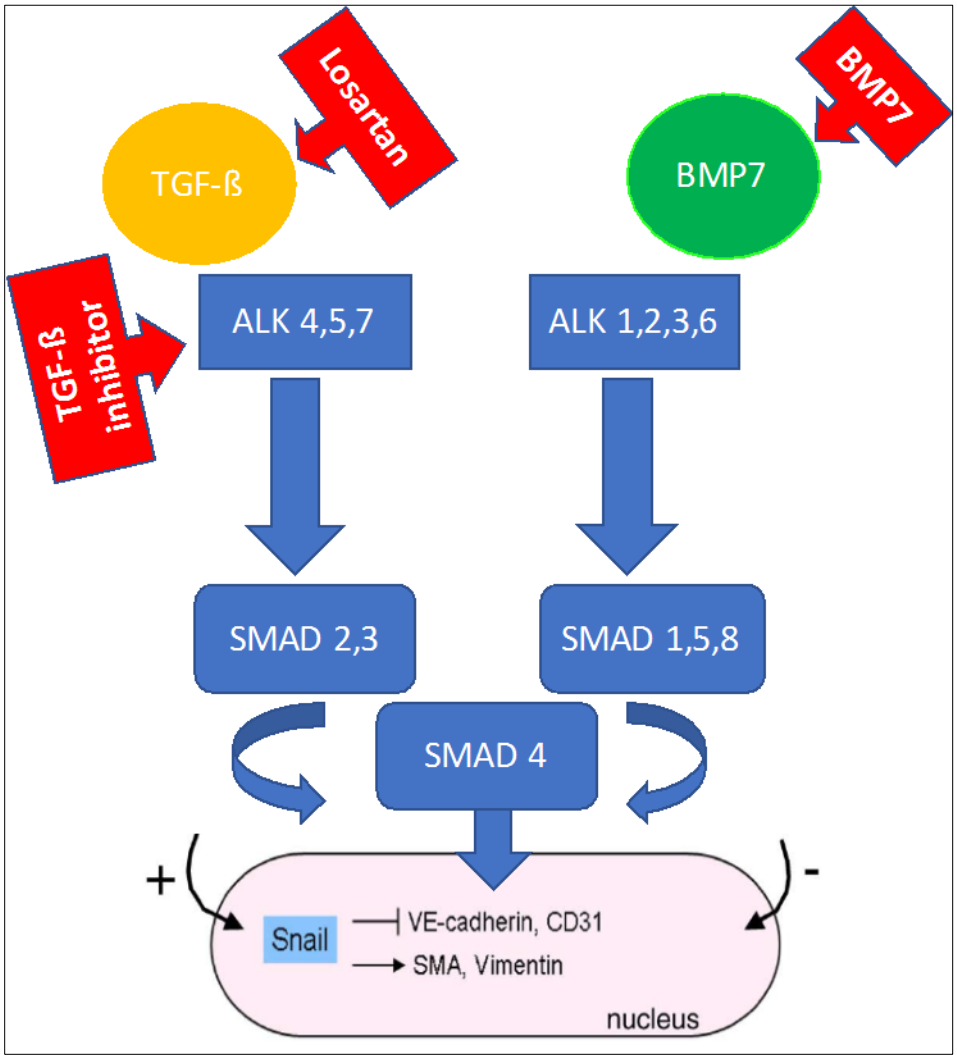

Figure 6: Different ways of TGF-ß inhibition. (© V. WEIXLER)

1.9. Aims of the Study

The aims of the study were to identify stimuli and regulator pathways leading to the development of EFE. The focus is on three different potential targets, which were selected according to clinical observations.

1. Is the development and progression of EFE formation an age-dependent process?
2. Do hemodynamic alterations lead to changes in shear forces such as lack of flow or turbulent flow trigger EFE formation?
3. What role do mechanical forces such as distension of the LV play in the formation of EFE?

Furthermore, I was interested whether the above-mentioned triggers limited fibrosis to the endocardium or also involved the myocardium as a consequence of maturation of the heart. The ultimate goal, however, was to determine clinically applicable treatments through direct inhibition of regulatory pathway intermediaries.

2. Methods

The basis for this investigation is human EFE tissue, which is obtained during routine surgeries where resection is performed as part of the surgical procedure. More detailed analysis was performed on this tissue.

In order to pursue the above-mentioned aims, we used three different models:

1.) an *in vitro* endocardial endothelial cell culture model: This model allows for isolated determination of alterations in flow or strains, respectively, on EndMT activation and regulation as well as inhibitor testing.

2.) an *ex vivo* whole heart preparation: A whole heart preparation according to retrogradely perfused Langendorff system was used to determine alterations in strain on endocardial and myocardial EndMT and the effect of age. This set-up was also used for inhibitor testing.

3.) Analyzing human EFE tissue: The concept of EndMT formation is studied in application of knowledge obtained from the animal models.

2.1. In-vitro Cell Culture Models

I used an already established cell culture model of endothelial cells (human coronary artery endothelial cells = HCAEC) but also refined an isolation method to use endocardial endothelial cells isolated from immature rat hearts (REEC) This model allows for isolated determination of alterations in flow or strains, respectively, on EndMT activation and regulation as well as inhibitor testing. Furthermore, different TGF-ß inhibitors and clinically applicable therapies such as Losartan were tested.

2.1.1. Cell Types

Human Coronary Artery Endothelial Cells (HCAEC)

As HCAEC have overlapping embryonic originate as endocardial endothelial cells (EC) (57), HCAE cells isolated from the right and left coronary arteries, purchased from Lonza (Cat. No.: CC-2585) were used at the beginning since they are an established cell culture model for EndMT studies. The cells were delivered in cryopreserved vials (>500.000 cells/vial) and either stored in liquid nitrogen for long-term storage or in a -80°C freezer for short-term storage until use.

Rat Endocardial Endothelial Cells (REEC)

To demonstrate that endocardial endothelial cells behave the same as coronary endothelial cells, REEC were isolated from 1-week-old neonatal rat pups. A litter (moms with 8-10 1-week-old-pups) was purchased from Charles River. Only the pups were used for isolating the REEC, the mom was euthanized with CO_2. After sedation with isoflurane for approximately 5 minutes, the hearts of the pups were removed and the left ventricle was dissected. After dissection, the surface of the left ventricle was rinsed with phosphate buffered saline (PBS) and afterwards incubated in little petri dishes containing 2 mg/ml collagenase for 20 minutes in a humidified incubator with 5% CO_2 at 37º C. After 20 minutes, the endocardial surface was gently scraped and then rinsed with PBS under sterile conditions (tissue culture hood). The solution was transferred into a centrifugation tube and centrifuged at 1200 rpm for 5 min. The supernatant was aspirated, the pellet was re-suspended in PBS and centrifuged again at 1200 rpm for 5 min. After aspiration of the supernatant the pellet was re-suspended in medium (EGM-2 growth medium) and cells were seeded on 6-well plates coated with 10 ug/ml fibronectin. REEC isolated from up to six hearts were pooled into one well of a 6-well culture dish. Cells were cultured at 37ºC under 5% CO2 in EGM2-MV medium. REEC identity was confirmed by positive staining for PECAM1 (endothelial marker) and negative staining for αSMA (mesenchymal marker). In the beginning the media was changed every 24 hours until the debris was gone and then changed every other day. Cells were passaged by trypsinization at a confluence of 70 to 80% and used for experiments at passage 1-3.

2.1.2. Growth Medium

For all endothelial cells EBM-2 Basal Medium purchased from Lonza (Cat. No.: CC-3156) supplemented with SingleQuot™ Kit from Lonza (Cat. No.: CC-4147) was used for cultivation. DMEM medium with additional 10% of fetal bovine serum (FBS) was used for centrifugation only (**Table 1 and 2**).

Item	Company/ Cat.No.
EBM-2 Basal Medium	Lonza/ CC-3156
SingleQuot™ Kit:	Lonza/ CC-4147
rhEGF (endothelial growth factor)	
GA-1000 (30mg/ml Gentamicin, 15g/ml Amphotericin-B)	
FBS 10%	
VEGF	
rhFGF-B	
R3-IGF-1	
Ascorbic Acid	

Table 1: EGM-2 MV growth medium contents

DMEM, high glucose, pyruvate	Gibco/11995-065
Fetal bovine Serum (FBS)	Gibco/10082147

Table 2: DMEM medium

2.1.3. Thawing of Cells

Six-well plates were initially coated with 1% sterile gelatin (5g gelatin dissolved in 500ml PBS and autoclaved for 30 minutes and filter-sterilized. After coating, the culture plates were covered with 1ml EGM-2 MV growth medium and placed in an incubator (37°C, 5% CO_2) for 30 minutes to equilibrate. Afterwards the frozen vial containing the cells was removed from the -80°C freezer and carefully thawed in a 37°C water bath until the last silver of ice melted. Cells were quickly transferred under sterile conditions (tissue culture hood) into a 15-ml tube and 9ml of DMEM medium was added. The tube containing the cells and the medium was centrifuged at 1200 rpm for 5 minutes. Afterwards the supernatant was aspirated and the remaining pellet was resuspended in EGM-2 MV growth medium. The solution was now transferred to the coated 6-well plates. Initially, cells from 1 vial (>500.000 cells) were seeded in two six-well plates until they reached 80-90% confluency and were then subculture. The plate was placed in the incubator (37°C, 5% CO_2) and media was initially changed every 24 hours after initiation of a new cell culture for

removal of all traces of dimethyl sulfoxide (DMSO) in the freezing media, and thereafter every other day (**Table 3**).

Item	**Company/ Cat.No.**
Gelatine from Bovine skin, powder, type B	Sigma-Aldrich/G9391
Sterile Phosphate Buffered Saline (PBS)	Sigma-Aldrich/P5368
Human Plasma Fibronectin Purified Protein	Millipore/FC010
6-well tissue culture plates	Olympus plastics/25-105
Barrier pipette tips 200ul, 1000ul	Genesee scientific/24-412, 24-430
Single Channel Pipettors	VWR
Electric Pipette	Drummond Scientific/108818
Serologic Glass Pipettes	Olympus Plastic/ 12-101/12-102/12-104
CO_2 Incubator	Symphony VWR 98000-386
Vortexer	VWR
Light Microscope	Nikon TMS/02747

Table 3: Materials for thawing the cells

2.1.4. Subculturing

Cells were sub-cultured after reaching 80-90% confluency and displaying many mitotic figures throughout the culture dish. Therefore, new culture dishes/plates were coated with 1% gelatin just like when thawing and seeding the cells for the first time. Pre-prepared coated culture 6-well culture plates were covered with 1ml of media and placed in the incubator for 30 minutes for equilibration. The culture dishes containing the cells were transferred from the incubator to the tissue culture hood and the existing media was aspirated. Afterwards the culture dishes were rinsed with PBS and afterwards covered with a trypsin/EDTA solution (for a $5cm^2$ culture dish/6-well plate 0.5ml trypsin/EDTA). Culture dishes were placed in the incubator for maximally 1 minute and afterwards gently trapped with the palm of the hand while observing under the light microscope until 90% of the cells were rounded up. Then media (2ml/$5cm^2$ culture dish) was added to stop the trypsinization process, and the solution was transferred to a 15ml tube adding media to reach a final volume of 9ml. Afterwards the tube was centrifuged at 1200rpm for 5 minutes. The

supernatant was aspirated and the pellet on the bottom of the tube was re-suspended with medium and transferred to the new culture dishes and placed in the incubator again (**Table 4**).

Item	**Company/ Cat.No.:**
Trypsin-EDTA (0, 25%)	Life technologies/25200-056

Table 4: Materials for Subcultering

2.1.5. Freezing of Cells

After reaching 80-90% confluency, cells were detached from original culture dishes by trypsinization using the same process as described before during the subcultering process. Instead of transferring, the cells were resuspended with EGM-2 medium after centrifugation, freezing medium was added (1ml/vial) and resuspended cells were quickly transferred to vials and frozen at a rate -1°C/min in the cryo-safeTM cooler. The frozen cells were stored in the -80°C freezer (**Table 5**).

Item	**Company/ Cat.No.:**
Synth-a-Freeze CTS	Gibco/A13713-01
Freezing Container, Nalgene Mr. Frosty	Sigma-Aldrich/ C1562-1EA

Table 5: Materials for Freezing the cells

2.1.6. Induction of EndMT in an *In Vitro* Cell Culture Model

a.) Uniaxial stretch cell culture model

My research group has already developed a cell culture model, in which it could be demonstrated that EndMT is activated by exposing HCAEC to uniaxial static stretch for several hours in special silicone stretch chambers purchased from Lifescience B-Bridge International Inc. (Cat. No.: ST-CH-04) mounted on a mechanical cell strain instrument (STREX B-Bridge International/ 140-10) (**See Figure 7**).

I used this already validated model to identify activation of pathways by mechanical strain to induce EndMT, to test different therapy options (BMP7, TGF-ß inhibitor SB431542 and Losartan) and establish each compounds therapeutic range.

Therefore, stretch chambers were coated with 10ug/ml fibronectin and cells were seeded in the center of each stretch chamber and covered with 3ml EGM-2 medium. When they reached 80-90% confluency, they were exposed to uniaxial stretch 10% of their original length for 8 hours in the 5% CO_2 incubator at 37°C. As a control, a stretch chamber was kept in a petri dish in the same incubator without exposure to stretch. After 8h stretch, the cells were fixed with 3.2% paraformaldehyde (PFA), diluted 32% paraformaldehyde in PBS) and afterwards treated with immunofluorescence staining, which is further described in the in the part "Immunofluorescence Staining" (**Table 6**).

I used 3 different groups: control (group 1), stretch only (group 2) and stretch+EndMT inhibition (group 3).

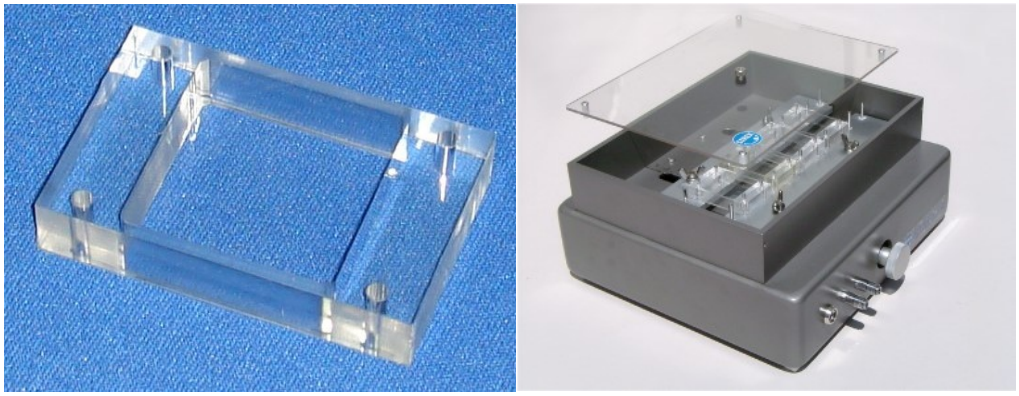

Figure 7: Stretching endothelial cells using stretch chambers (left) and STREX mechanical cell strain instrument (right) by Lifescience B-Bridge International.

Item	**Company/Cat.No.:**
stretch chambers	B-Bridge International/ ST-CH-04
mechanical strain apparatus	STREX B-Bridge International/ 140-10
Paraformaldehyde 32%	Electron Microscopy Sciences/15714-S

Table 6: Materials for the stretch chamber in-vitro model

b.) Establishing a shear stress cell culture model as proof-of-concept

Secondly, to test the hypothesis whether changes in shear forces induce EndMT, I established a shear stress cell culture model as a proof-of-concept. A flow chamber model was created which allowed alterations in flow patterns followed by determination of stimulation of EndMT and regulation.

For this purpose, ECs were grown on cover slides (diameter 12mm) in 24-well culture dishes, coated with 1% gelatin and covered with EGM-2 MV medium until they reached 80-90% confluency. Afterwards the cover slides were gently removed from the 24-well plates and inserted in a therefore designed flow chamber and perfused there for 3h at 37°C in the incubator (**Table 7**).

The flow chamber, which was designed and build for this experiment originally consisted of a small container with two holes drilled on both sides, connected to tubing and with small a pedestal in the center of the container, which served as a "slide holder" as the cover slide with the cells was fixed on top with adhesive tape. The container and the tubing were covered with growth medium and the tubing was connected to a roller pump (Masterflex Pump System). The flow chamber was then adjusted several times and different flow speeds (gpm=gallons per minute) were applied in order to force the EC to laminar vs. a turbulent flow. Based on the pump speed (Q in gpm), the cross-sectional area (A) of the container (water depth x length of container) we were able to calculate the sheer forces (τ), the EC were exposed to (58). I ended up using a flow rate of 5gpm, as this was comparable to the shear forces existing in the human blood vessels and the heart. (**See Figure 8 and 9**).

Item	**Company/ Cat.No.:**
PVC Tube 3/8x1/2" 100 feet	VWR/89068-512
Masterflex Console Drive L/S Model 7720062	Masterflex Pump System
24-well culture dishes	Olympus plastics
Fisherbrand Microscope Cover Glass 12mm	Fisher Scientific/ 22-293232

Table 7: Materials for flow chamber in-vitro model

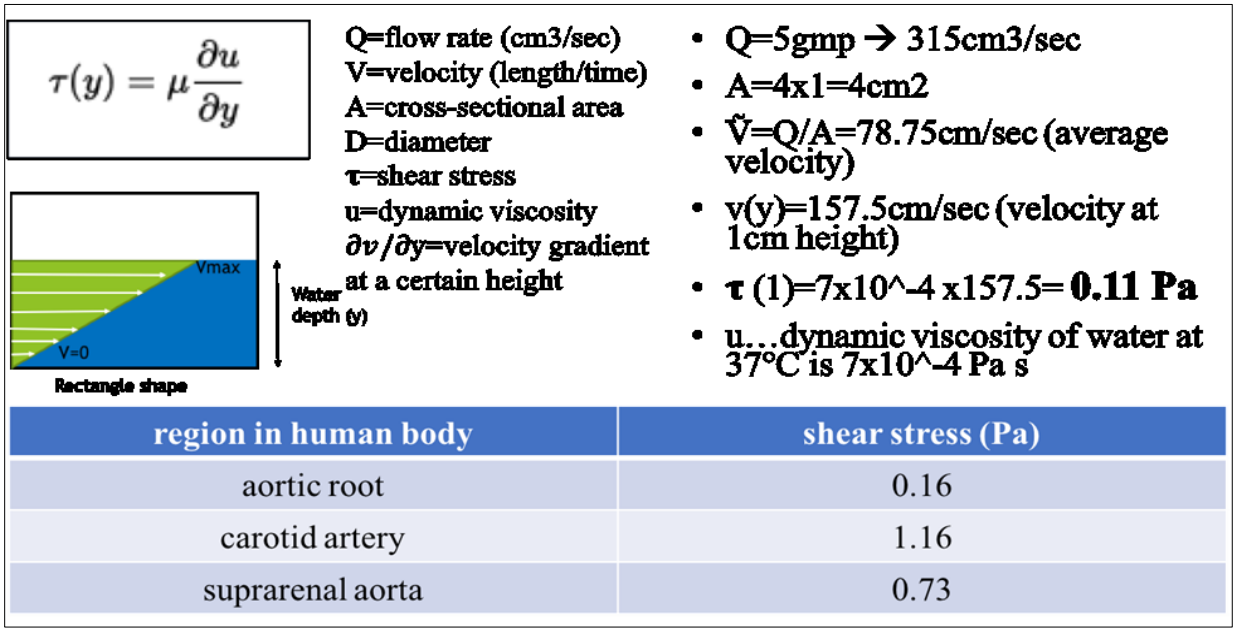

region in human body	shear stress (Pa)
aortic root	0.16
carotid artery	1.16
suprarenal aorta	0.73

Figure 8: Calculation of shear forces at a given pump speed (Q) and water depth (y). (© V. WEIXLER)

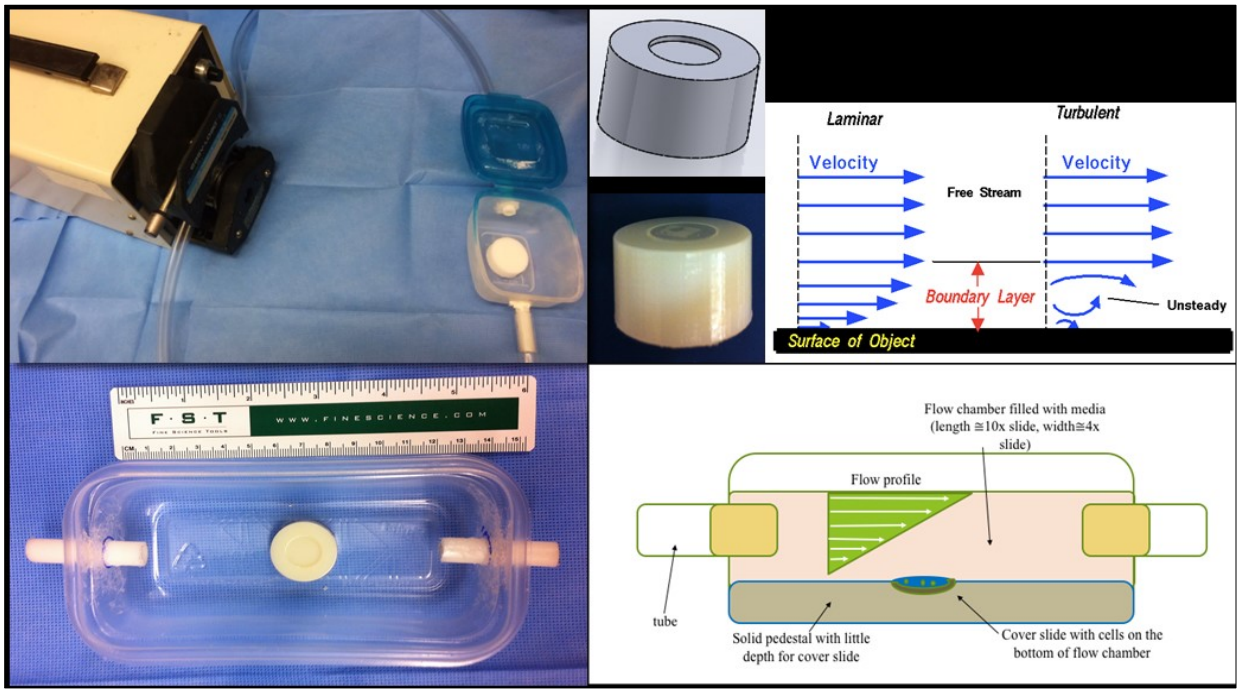

Figure 9: Self-designed flow chamber with slide holder in the center with Masterflex pump system (above). (© V. WEIXLER)

c.) Induction of EndMT with recombinant TGF-ß

Induction of EndMT with TGF-ß is a well-established method (59) and was used as positive control for our cell culture models. TGF-ß1 was purchased from R&D systems and as an extremely hydrophobic protein, it needs to be reconstituted at 20 ug/ml in 100ul sterile 4mM HCl containing 1mg/ml bovine serum albumin. The cells were cultivated on cover slides (12mm) in 24-well plates first until they reached 80-90% confluency and then starved with growth medium diluted with EBM-2 basal medium (1:10 dilution) and with 10ng/ml TGFß1 for 12 hours (31) (**Table 8**).

Item	**Company/Cat.No.:**
Recombinant human TGF-ß1	R&D systems/240-B-002

Table 8: Materials for direct inducing EndMT with TGF-ß1

2.1.7. Inhibition of EndMT

Cells cultured in stretch chambers as well as cells on cover slides exposed to flow, were treated with 3 different EndMT inhibitors working on different positions of the TGF-ß pathway: BMP-7, a TGF-ß specific inhibitor or Losartan. The *in vitro* cell model was used to find the right concentration for each treatment for further use in the *ex vivo* and *in vivo* models. The concentration shown in Table 9 are the final working concentrations, which indicated a significant decrease in the number of double-stained endocardial cells without losing cells due to toxic side-effects. All reagents were administered contained in a gelatin sponge which was incubated together with the cells in cell culture media. This application method was used to mimic potential localized administration *in vivo*. To ascertain that gelatin had no effect on EndMT, a control cell culture experiment was performed, where unstimulated cells were exposed only to the gelatin sponge (**Table 9**).

Reagent	**Company/Cat. No.**	**Concentration**
Recombinant human BMP-7	Gibco/PHC7204	10ng/ml
TGF-ß inhibitor SB431542	Tocris/CAS 301836-41-9	10uM
Losartan potassium	Santa Cruz/CAS 124750-99-8	5uM-10uM
Gelfoam®Absorbable Gelatin Sponge, USP	Pharmacia&Upjohn Company 09-0396-05	

Table 9: Inhibiting EndMT

2.1.8. Determination of EndMT

As already described, EndMT is the process of endothelial cells losing their cell-cell contacts and transforming into migratory mesenchymal cells. During this process, endothelial cells lose their endothelial markers such as CD31/PECAM1/VE-cadherin and acquire mesenchymal markers such as FSP1 and α-SMA. The standard method to verify active EndMT is, thus, immunofluorescence staining. Double staining of a cell with both markers is evidence for active EndMT. Primary antibodies against endothelial markers (PECAM-1/CD31, VE-cadherin) and against mesenchymal markers (α-SMA) were used. Secondary antibodies conjugated to the red-fluorescent Alexa-647 or green-fluorescent AF-488 were used. The nuclei were stained with blue fluorescent 4',6-diamidino-2-phenylindole (DAPI nuclei acid stain).

The underlying concept of immunofluorescent staining is to detect specific antigens, in our case endothelial and mesenchymal markers by first binding a primary antibody (1ry AB) to it, which binds the target molecule and then making this target molecule visible by linking a secondary antibody (2ry AB) which contains a fluorescent marker, to the primary antibody. In order to block non-specific binding sites, a blocking buffer containing normal serum from the same host species as the labeled secondary antibody is used. For the 2ry AB we used (AF 488 and Texas Red Mouse) normal horse and normal donkey serum was used to prepare the blocking buffer (250ul normal donkey, 250ul normal horse serum in 950ul PBS) or bovine serum albumin (0.15g BSA in 10ml PBS) was used as universal blocking buffer additive.

a.) Immunofluorescence staining of cultured cells

Cells grown in stretch chambers and cells grown on cover slides in flow chambers were washed with PBS and fixed with 3.2% PFA at the end of the experiments. After fixation for 15 minutes, cells were washed with PBS again and afterwards 0.2% Triton X-100 was applied for 10 minutes followed by another washing step with PBS and incubation with blocking buffer containing the primary antibodies in the concentrations recommended by the respective companies for 1 hour. Then another wash with PBS was performed, and cells were incubated again for 1 hour with blocking buffer solution containing the secondary antibodies. During the staining process cells were incubated in the dark preventing light exposure to prevent bleaching of fluorescence. After another wash with PBS and distilled

water, cells were mounted with mounting medium, either directly on the stretch chambers or mounted onto microscopic slides (**Table 10, 11 and 12**).

Item	**Company/ Cat.No.:**
Triton X-100	SIGMA/X100-500ml
Mounting Medium	Dako/ S3025
Microscopic Slides	VWR/ 16004-422

Table 10: Immunofluorescent Staining

Item	**Company/Cat.No.:**
Bovine Serum Albumine (BSA)	Sigma Aldrich/ A7906
Normal Donkey Serum	Jackson Immuno Research/ 017-000-121
Normal Horse Serum	Jackson Immuno Research/ 008-000-121

Table 11: Blocking Buffer

Primary Antibody (1ry AB)	**Company/Cat.No.**	**Concentration Ab:BB**
PECAM-1 (goat)	Santa Cruz/sc-1506-R	1:50
α-SMA (mouse)	Sigma Aldrich/A2547	1:400
twist (H-81, rabbit polyclonal)	Santa Cruz/sc-15393	1:50
SLUG antibody (H-140, rabbit polyclonal)	Santa Cruz/ sc-15391	1:100
Secondary Antibody (2ry AB)	**Company/Cat.No.**	**Concentration Ab:BB**
Alexa Fluor 488 (donkey anti-goat)	Life Technologies/A11034	1:200
Alexa Fluor 647 (horse anti-rabbit)	Invitrogen/A32733	1:200
Texas Red Anti-Mouse IgG	Vector Laboratories/TI-2000	1:100
DAPI	Molecular Probes/D1306	1:1000

Table 12: Antibodies for Immunofluorescent Staining

b.) Visualization

Following immunofluorescent staining, slides were stored in the dark in the refrigerator at +4°C. Slides were then analyzed with a Zeiss Observer.Z1 fluorescent microscope with a Nikon 10x objective, NA=10x/0.25 and 20x objective, NA=20x/0.45, respectively. Double staining for endothelial as well as mesenchymal markers was identified as active EndMT. Ten randomly selected fields from each slide were photographed with a Leica digital colour camera and analyzed. First the total cell count was determined through automatic counting (ImageJ), then double stained cells were counted by hand by two blinded investigators.

2.1.9. Endothelial cell viability

To confirm that endothelial cells were still functional according to their phenotype, I used Dil complex acetylated low-density lipoprotein (Dil-Acetylated-LDL) from human plasma (Thermo Fisher, Waltham, MA) which is only internalized by viable endothelial cells and fluoresces upon uptake. Mesenchymal cells do not internalize this compound and thus, it allows for endothelial cells with respective characteristics to be distinguished from mesenchymal cells (**Table 13**).

Item	**Company/Cat.No.:**
Low Density Lipoprotein from Human Plasma, acetylated Dil complex (Dil AcLDL)	ThermoFisher Scientific/ L2484

Table 13: Endothelial cell viability

2.2. *Ex vivo* Isolated Heart Model (Langendorff System)

In order to translate the findings from an isolated cell culture model to an entire organ, I decided to use a whole heart preparation to validate our cell culture data. With extensive experience with the isolated Langendorff heart model in the lab, a set-up was created to perfuse immature and mature rat hearts retrogradely for 3 hours and to expose those hearts to maximal degree of mechanical forces through a weight attached to the apex of the LV. The advantage of this model is also that testing new treatment options on the myocardium is possible without neuronal or humoral influences.

2.2.1. Langendorff System

The non-working Langendorff model is designed for a freshly isolated heart to be retrogradely perfused through the ascending aorta. Coronary arteries are perfused directly with modified Krebs-Henseleit solution, oxygenated with 95% oxygen, at a constant temperature of 37°C. The Langendorff apparatus therefore consists of a reservoir for the Krebs-Henseleit solution, an oxygen tank, a heating coil and perfusion cannulas. This allows the isolated hearts to continue beating for several hours outside the animals' bodies (**Table 14**).

Krebs-Henseleit solution	**Concentration in mM/L**
Glucose	11.5
NaCl	118
$NaHCO_3$	23.5
$MgSO_4$	2.4
KH_2PO_4	1.2
KCl	3.3
10% $CaCl_2$ (10g $CaCl_2$ in 100ml distilled water)	9.1

Table 14: Krebs-Henseleit Solution

2.2.2. Ex-vivo Heart Model

As the purpose of this experiment was to determine whether mechanical forces induce EndMT in endocardial and endothelial cells in the heart and not only in isolated cells. Furthermore, the impact of age on this mechanism was determined assuming that maturation involves the remodelling of the extracellular skeleton and preventing from EndMT to be induced. Therapeutic compounds successfully tested in cell culture were now applied to this whole heart preparation.

All rats were weighed first and then anaesthetized with isoflurane (0.5-2%) in an acrylic induction chamber. The hearts were quickly removed from the animals through a v-shaped cut along the ribs and transferred with a minimum time of delay into Krebs-Henseleit solution, which was kept on ice. The ascending aorta was cut as distally as possible, lungs as well as other vessels were removed. Before cannulation, the hearts were weighed and then the aorta was cannulated with a 16-G steel cannula and the heart mounted onto the Langendorff apparatus. Hearts, which were

forced to mechanical strain, were exposed to a weight 10x the heart weight, which was fixed with a Prolene 5-0 suture onto the apex. Hearts were then kept warm and perfused for 3 hours. After 3 hours, effluent from each heart was collected for 1 minute and frozen (-80°C) for further investigation. Hearts were conserved in 5ml tubes filled with 4% formalin until paraffin slides were obtained (**Table 15 and Figure 10**).

Item	**Company/Cat.No.:**
Intramedic Tubing Adapters 16-Gauge	Fisher Scientific/22-044083
2L Water Jacketed Reservoir	Radnoti/120142-2
Heating Coil 5.5ml	Radnoti/158822

Table 15: Langendorff apparatus

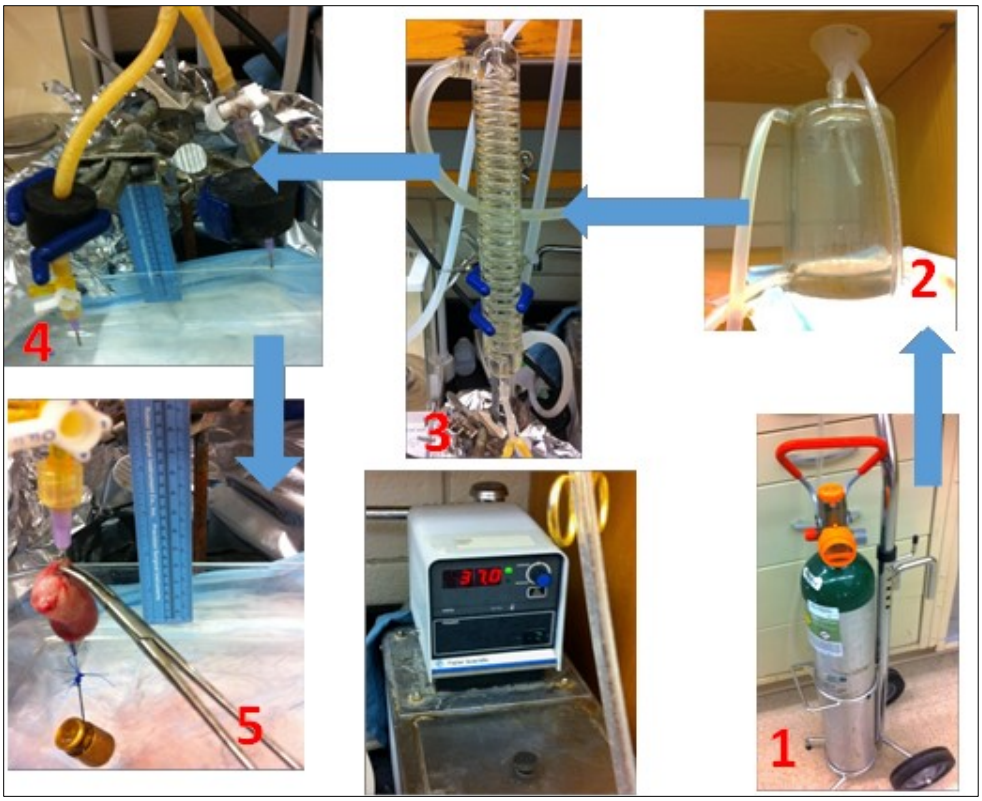

Figure 10: Langendorff apparatus: 1=oxygen tank, 2= reservoir of perfusate, 3=heat exchanger, 4=perfusion cannulas, 5=perfused heart with mechanical strain. (© V. WEIXLER)

2.2.3. Inhibiting EndMT in Stretched Rat Hearts

Three different EndMT inhibitors (BMP7, TGF-ß inhibitor SB-431542 and Losartan) were selected based on the cell culture experiments and compounds were applied either locally via a gelatin sponge, which was inserted through the left appendage into the left ventricle (**See Figure 11**) or systemically directly given via Krebs-Henseleit solution, respectively. For local application, the heart was perfused with fresh Krebs-Henseleit perfusion out of a 2L reservoir, which was used for a one-time passage through the coronary system of the heart.

For systemic perfusion, a smaller reservoir (250ml) was used and the working concentration of Losartan (5-10uM) was added directly to the solution. After flushing the heart, the solution was collected in a glass funnel and pumped back with a roller pump to the reservoir for recirculation of Losartan (**Table 16**).

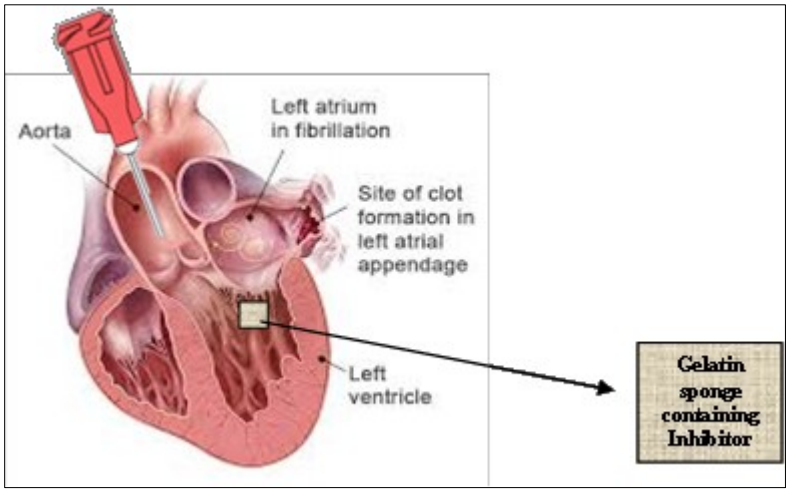

Figure 11: Local application of different inhibitors via a gelatin sponge. (© V. WEIXLER)

Item	**Company/Cat.No.:**
250ml Water Jacketed Reservoir	Radnoti/120142-025
Reservoir Filling Glass Funnel	Radnoti/120140-A
PVC Tube 3/8x1/2” 100 feet	VWR/89068-512
Masterflex Console Drive L/S Model 7720062	Masterflex Pump System

Table 16: Systemic application of Losartan in Langendorff system

2.2.4. Experimental groups

The following 5 groups were evaluated:

1.) Group 1: control (perfusion only)
2.) Group 2: weight only (perfusion+weight)
3.) Group 3: weight+ local BMP7 (perfusion+weight+local BMP7)
4.) Group 4: weight+local TGF-ß inhibitor (perfusion+weight+local TGF-ß inhibitor)
5.) Group 5: weight+ local Losartan (perfusion+weight+local Losartan)

A total of 62 hearts were perfused for 3 hours. Each group included 7 immature hearts (rats <100g, rat hearts< 1g) and 5 mature hearts (rats>100g, rat hearts>1g).

2.2.5. Using FITC Lectin to Label Endothelial Cells

Because of strong background staining for CD31, it was difficult to determine the number of endothelial cells within the myocardium accurately. Therefore, FITC lectin from Lycopersicon esculentum (tomato) was applied at the end of the 3h-perfusion in order to label all endothelial cells prior to the immunofluorescent staining process as our research group has already shown before (60,61). Lectin binds onto the surface of endothelial cells and can therefore be used to determine myocardial microvascularity. A concentration of 20ul/ml of FITC-lectin was dissolved in PBS and a total amount of 10ml solution was injected directly into the coronary vessels at the end of the experiment over 5 minutes. Afterwards the hearts were fixed in 4% formalin and stored in the dark until sectioning. Following sectioning, slides were stained with alpha-SMA and DAPI (**Table 17**).

Item	**Company/Cat.No.:**
FITC lectin from Lycopersicon esculentum (tomato)	Sigma Aldrich/L0401-1mg

Table 17: Using FITC Lectin to label EC

2.2.6. Histological Slides and Staining

Immunofluorescent staining was then performed on unstained slides with antibodies directed against alpha-SMA, PECAM-1/CD-31 as well as different transcription factors (twist, SLUG/SNAIL) as described above in the section "Immunofluorescent Staining".

Double-staining for both, endothelial and mesenchymal markers validated active EndMT. Ten randomly chosen sections in the endocardium as well as the myocardium of the left ventricle were photographed. Total cell count was calculated with ImageJ and two independent blinded investigators counted the double stained cells in each picture. Statistical analysis, comparing the ratios (double stained cells/total cell count) in each group using ANOVA followed by Bonferroni post-hoc correction, was performed with SPSS software.

2.3. Analyzing Human EFE tissue

2.3.1. Patients

EFE tissue from a total of 24 patients was analyzed, who were diagnosed with HLHS at Boston Children's Hospital and who underwent surgery with EFE resection from December 2011 to March 2018.

Out of these 24 HLHS patients, tissue from 17 patients was sent as 'de-identified discarded tissue', resected during open heart surgeries and tissue from additional 6 patients, in whom consent was obtained prior to the surgery. In the latter group, we followed the patients collecting clinical background and imaging data, and obtained EFE tissue from previous resections if available.

Six patients were included for comparison with diagnoses other than HLHS but with known flow disturbances across aortic (AV) and/or mitral valve (MV). In all of these patients, preoperative standard imaging studies (echocardiography and MRI) did not describe EFE. Macroscopic appearance of "EFE-like tissue" in the LV outflow tract diagnosed by the treating cardiac surgeon led to resection of endocardial tissue in the operating room.

As controls, I received two de-identified discarded tissue samples from the right ventricle (RV) from patients without flow disturbances, which was resected in both cases because a right ventriculotomy was performed during the surgical procedure. Furthermore, a healthy rat LV was used as negative control.

All tissue samples, once received from the operating room were immediately embedded in optimal cutting temperature (OCT) compound, snap frozen and stored at -80°C for future analysis. Frozen sections were produced from OCT blocks and further processed for microscopic analysis as described in more detail below (**Table 18)**. All EFE tissue received contained some degree of myocardial infiltration (62).

Item	**Company/Cat. No.:**
OCT compound	Fisher healthcare/ 23-730-571
2-Methylbutane	Sigma Aldrich/M32631

Table 18: Embedding and freezing of human EFE samples

2.3.2. Presence of EndMT:

To demonstrate that the resected tissue contained active EndMT, I performed immunohistochemical staining for the endothelial marker CD31 (1:100, Dako) as well as for the mesenchymal marker alpha-SMA (1:100, Abcam). Double staining for CD31 and alpha-SMA indicated EndMT. Additionally, all samples were stained for the transcription factors TWIST (1:100, Abcam) and SLUG/SNAIL, which as described above, are part of the transcription regulation pathway of EndMT. A TWIST or SLUG/SNAIL-positive stained nucleus was rated also EndMT-positive. Nuclei were stained for DAPI (1:1000) (**Table 19**) (31,62,63).

Item	**Company/Cat. No.:**
Alpha-SMA	Abcam/ ab32575
CD31	Dako/ M0823
Anti-twist 1	Millipore/ ABD29
Alexa Fluor 488 anti-rabbit	

Table 19: Immunofluorescence staining for EndMT

2.3.3. Assessing the Composition of EFE Samples

Age-related changes of EFE tissue were examined for the amount of collagen and elastin, vascularity, and cellularity by staining with H&E, MT and Elastin. All slides were visualized using a Zeiss Observer.Z1 fluorescent microscope with a Nikon 20x objective (NA=20x/0.45). Ten randomly selected fields from each slide were taken and quantification was performed with ImageJ (version 2.0.0-rc-43, obtained from the National Institute of Health, Bethesda, MD) (62,63).

2.3.4. Analysis of the Myocardium in EFE Samples

As all the samples contained some degree of muscle tissue from the underlying myocardium, also the myocardium was analyzed for EndMT-positive tissue and the cardiomyocytes were stained for desmin (1:50, Abcam), which is a major intermediate filament protein in cardiac, skeletal and smooth muscle and is essential for structural integrity and function in a healthy muscle (62–64) (**Table 20**).

Item	**Company/Cat. No.:**
Anti-Desmin antibody	Abcam/ ab8592

Table 20: Immunofluorescence staining for Desmin

2.3.5. Determination of Enzymatic Degradation of the Extracellular Matrix through In Situ Zymography

To determine whether the increased deposition of collagen and elastin is a consequence of impaired proteolytic enzymes activity, I performed a "*in situ* zymography", which is a technique to visualize the proteolytic activity of enzymes such as matrix metalloproteinases (MMPs) degrading extracellular matrix (ECM) components. The focus was on MMP2/9, gelatinases degrading collagen and MMP12, elastase which breaks down elastin. Therefore, a substrate (DQ Elastin, DQ Gelatin) is applied on either fresh tissue or frozen sections and incubated. If elastase/MMP activity is present in the samples, green fluorescence can be visualized through a fluorescence microscope (**Figure 12**).

I was especially interested to see if there are differences in human EFE samples obtained from different age groups.

For elastase activity, the sections were removed from the -80°C freezer and thawed at room temperature for a few minutes. Afterwards the sections on the glass slides were marked using a liquid blocker pen and then incubated at 37°C in a wet chamber with DMEM containing 10% FBS and supplemented with FITC conjugated DQ Elastin (40ug/ml) for 1 hour. As negative control one slide was incubated with DMEM+10% FBS only at the same conditions. Afterwards sections were washed 3x in PBS and then counterstained with Tropoelastin and DAPI.

For gelatinase activity, cryosections were also removed from the freezer and then incubated at room temperature for 10 minutes with incubation buffer consisting of 50mM Tris pH 7.4, 150 mM NaCl and 5mM CaCl2. Afterwards sections were marked with liquid blocker pen and covered with 200ul incubation buffer supplemented with FITC conjugated DQ Gelatin (50ug/ml) for 16h at 37°C in a wet chamber. Afterwards sections were washed 3x in PBS and counterstained for DAPI and collagen 1. A negative control was incubated with an incubation buffer containing 10mM EDTA instead of CaCl2 and without DQ Gelatin (62,63,65,66) (**Table 21**).

Item	**Company/Cat. No.:**
DQ Elastin (EnzCheck Elastase Assay Kit)	Thermo Fisher/E12056
Anti-Tropoelastin antibody	Abcam/ ab21600
DQ Gelatin (EnzCheck Gelatinase/Collagenase Assay Kit)	Thermo Fisher/ E12055
Collagen 1	

Table 21: In situ zymography: Measuring Elastase/ MMP activity

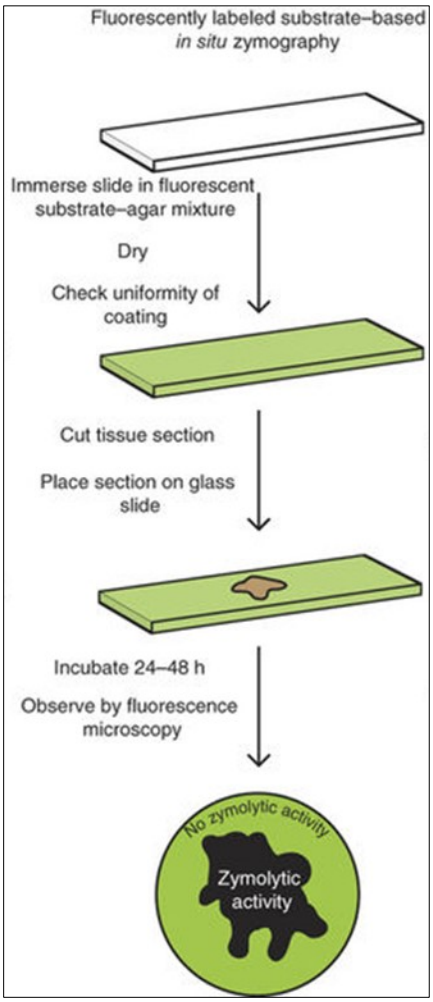

Figure 12: Technique of in-situ zymography. Reproduced from Vandooren et al. (2013) with permission of Nature Publishing Group.

2.3.6. Clinically relevant background information:

After obtaining consent in a sub-group of HLHS and non-HLHS patients, I was able to associate prior EFE resections, imaging data and other clinically relevant information to the histological findings (62,63).

3. Results

3.1. In-vitro Cell Culture Model

3.1.1. Stretch Chamber

After exposure to 10 % of static uniaxial stretch for 8 hours, HCAECs in group "stretch only" lost their typical cobblestone morphology typical for endothelial cells and showed significant more double-stained (staining for both, PECAM-1 and α-SMA) cells indicating EndMT (46±13% of total cell count) compared to group "control" (7±2% of total cell count); P=0.05. When BMP7 was added to the stretch chamber (group "stretch+BMP7"), HCAECs retained their endothelial phenotype and significantly less double-stained cells were observed compared to stretch and with similar counts as in controls (7±2% of total cell count); but differed significantly (P<0.001) from the group 'stretch only'. To confirm these results, Dil complex acetylated low-density lipoprotein from human plasma was used which is only internalized by viable and phenotypical endothelial cells and fluoresces upon uptake (**Figure 13 and 14**). These results suggest that static stretch induced EndMT is regulated through activation of the TGF-β pathway which was shown by direct inhibition with the TGF-ß specific inhibitor (SB431542). With future clinical use in mind, I also tested BMP7 and Losartan as inhibitors after establishing that stretched endothelial cells undergo EndMT through activation of the TGF-beta pathway. The TGF-ß inhibitor SB431542, applied on stretched EC, was successfully inhibiting EndMT when used concentrations of 10uM and was toxic at concentrations >100uM. For Losartan we established a concentration range of >5uM and <10uM (67).

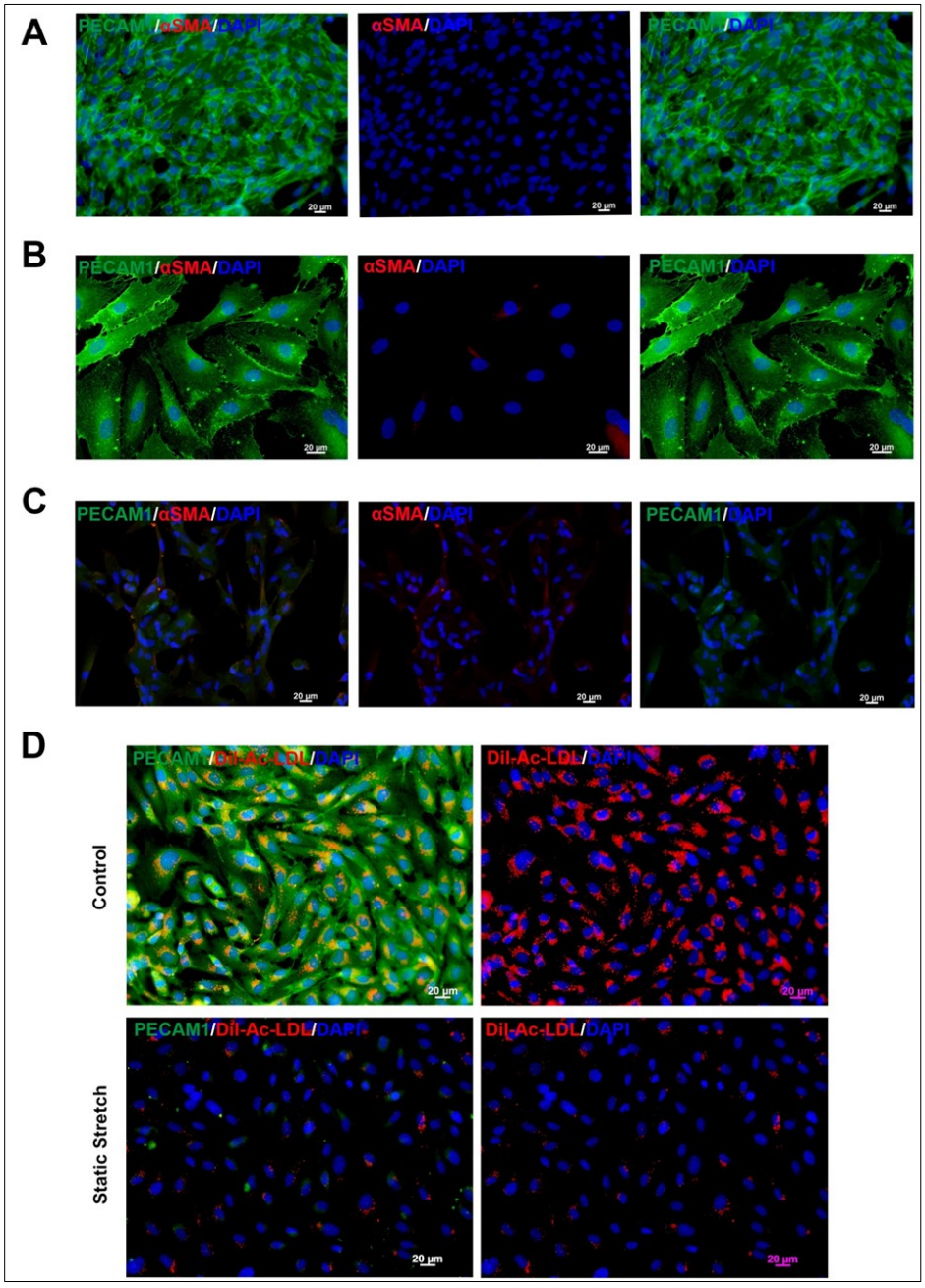

Figure 13: (A) HCAEC present with cobblestone morphology typical for endothelial cells. (B) and (C) Representative histological sections of control ECs and stretched ECs are shown. Both slides were stained with the EC marker, PECAM1 (green), the mesenchymal marker, αSMA (red), and nuclei in blue (DAPI). ECs in the control picture only stained for the EC marker PECAM1 indicative of the endothelial phenotype. In comparison, stretched ECs were positive for both markers. Double-staining with an EC and a mesenchymal marker is indicative of active EndMT. (D) To confirm the results of stretch-induced EndMT in HCAEC, we added the functional endothelial marker Dil complex acetylated Low Density Lipoprotein (Dil-Ac-LDL) to the media of the cell culture dish. Dil-Ac-LDL (red) is only internalized by endothelial cells and fluoresceces upon uptake. As indicated by the representative pictures, stretched cells had no functional ECs compared to the ECs (green) in the control group. (© V. WEIXLER)

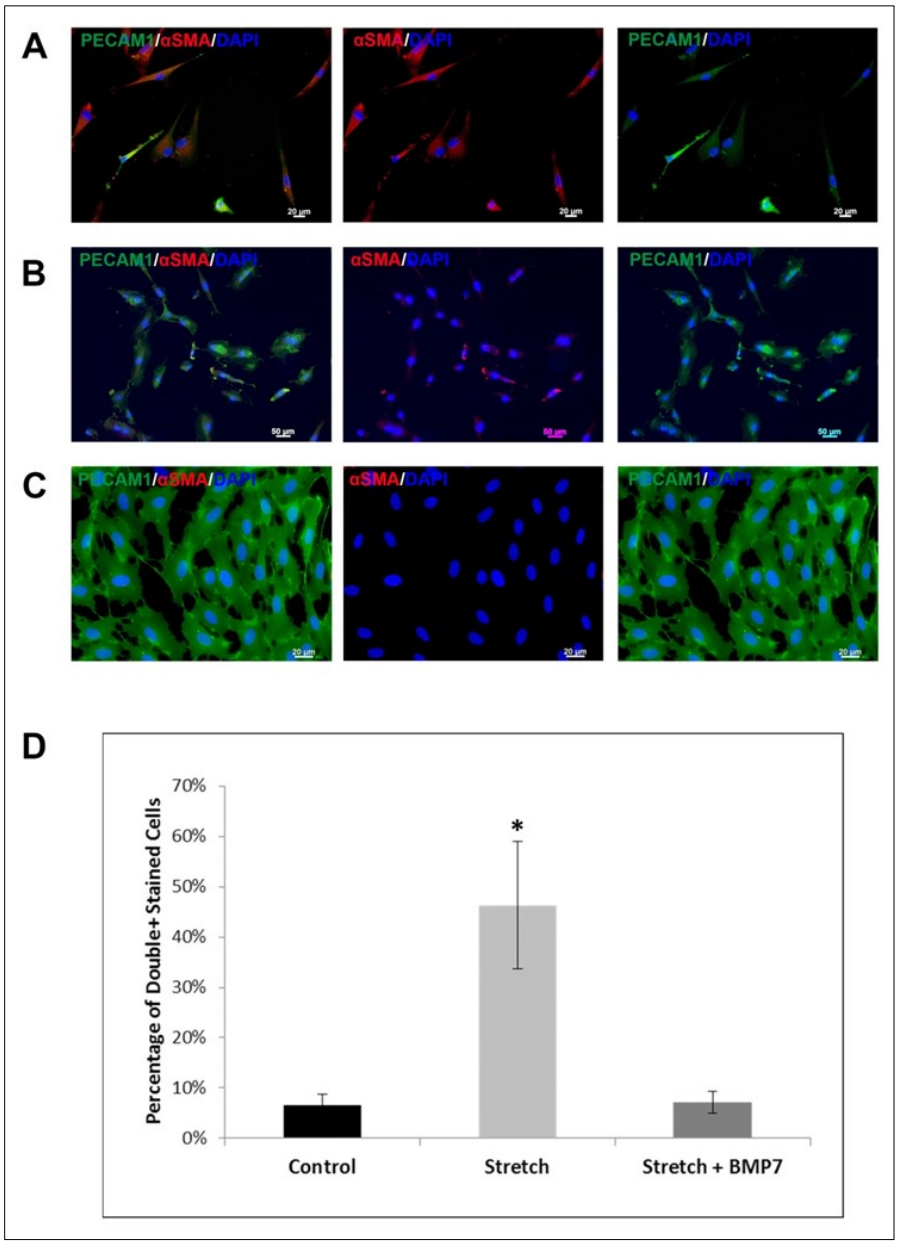

Figure 14: Stretch-induced EndMT is mediated by activation of the TGF-β pathway which is shown by representative immunohistochemical pictures where double-staining of ECs with an endothelial cell maker (PECAM1 in green) and a mesenchymal marker (αSMA in red) is indicative of active EndMT.(A) ECs exposed to TGF-β served as positive control for active EndMT. (B) ECs exposed to 8 hours of uniaxial stretch underwent EndMT. (C) When BMP-7 was added to ECs exposed to uniaxial stretch cells retained their endothelial morphology and only stained positive for the EC marker PECAM1. (D) Following BMP-7 treatment, significantly less cells stained for both the EC marker PECAM1 and the mesenchymal marker αSMA compared to the cells in the stretch chamber not containing BMP-7 as indicated by this graph. (© V. WEIXLER)

3.1.2. Flow Chamber

As the newly created *in vitro* flow chamber model was established as proof-of-concept for EndMT activation and inhibition, only preliminary results are available for these experiments. Perfusing ECs for 3h with a pump flow of 5gpm showed successful induction of EndMT on the edges of the cover slide, where turbulent flow pattern developed. In the center of the cover slide, however, where laminar flow was maintained, EC cells did not undergo EndMT (**Figure 15 and 16**).

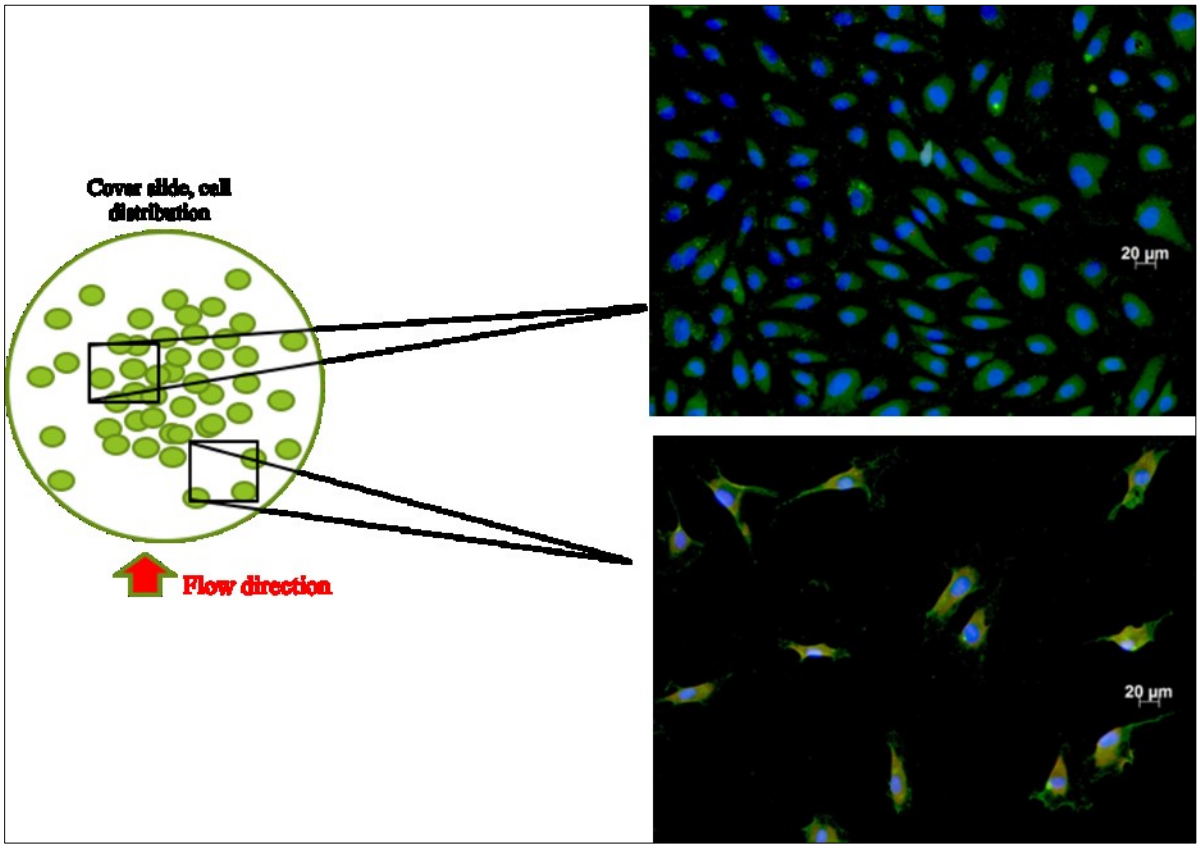

Figure 15: Cover slide with EC, after 3h in flow chamber, cells in center, exposed to laminar flow did not change their morphology, however cells on the edges of the cover slide, which were exposed to turbulent flow underwent EndMT and changed to mesenchymal cells, blue=DAPI, green=PECAM1, red=alpha-SMA, orange=double-staining. (© V. WEIXLER)

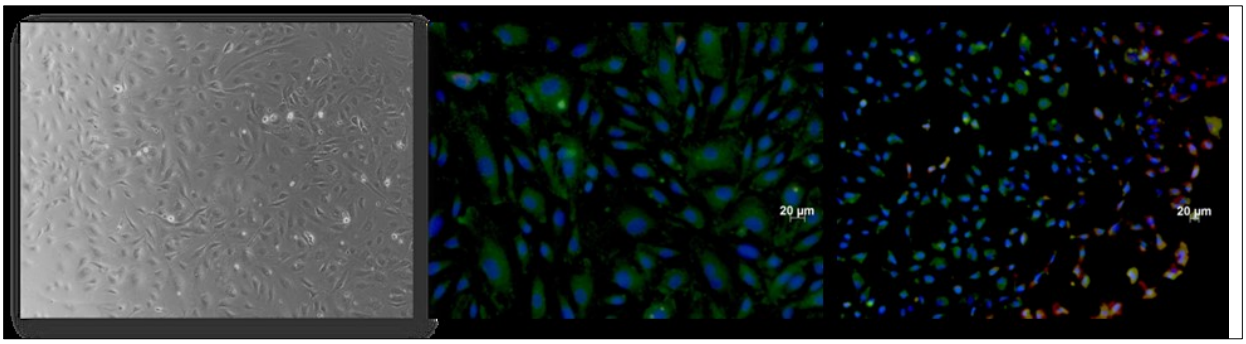

Figure 16: Forcing EC to laminar/turbulent flow in flow chamber; picture on the left: cells prior to exposing them to different flow pattern, picture in the middle: cells in the center staining for PECAM-1 only, picture on the right: cells on the edges of the cover slide are stained with PECAM-1 and alpha-SMA indicating EndMT. (© V. WEIXLER)

3.2.Ex-vivo Langendorff model

In this set of experiments, I determined EndMT induction and inhibition in the following groups: (each group contained 7 immature and 5 mature hearts)

1.) Group 1: control (perfusion only)

2.) Group 2: weight only (perfusion+weight)

3.) Group 3: weight+ local BMP7 (perfusion+weight+local BMP7)

4.) Group 4: weight+local TGF-ß inhibitor (perfusion+weight+local TGF-ß inhibitor)

5.) Group 5: weight+ local Losartan (perfusion+weight+local Losartan)

After exposing immature hearts to uniaxial stretch (10x of their heart weight) for 3 hours with constant perfusion on a Langendorff apparatus, significantly more double-stained (α-SMA /PECAM1) endothelial cells/total endothelial cells were found than in than control hearts which were only perfused (15.9%±2 vs. 3.1%±0.8, $P<0.01$). These results were confirmed by staining for the transcription factors SLUG/SNAIL downstream of the TGF-β pathway (control: 15.2%±3.3 versus stretch: 46.8%±3.7), which was significantly different ($P<0.01$)

To establish that inhibition of the TGF-β pathway can block EndMT, I locally applied BMP7, the TGF-ß inhibitor SB431542 or Losartan, respectively in uniaxial-stretched immature ex-vivo hearts. Following administration of either one of the three TGF-ß inhibitors, the ratio of α-SMA /PECAM1 double stained ECs was significantly lower (stretch+BMP7: 2.9%± 0.1,

stretch+SB431542: 5.2%± 1.3 and in stretch+losartan: 0.09%± 0.1) compared to hearts exposed to uniaxial stretch ($P<0.01$). Compared to controls, stretched hearts with one of the three TGF-ß inhibitors were not significantly different ($p>0.05$). Only group 1 (weight only_immature) had significantly more ($P<0.05$) double stained (PECAM1/αSMA) endothelial cells indicating EndMT than all the other groups. The control and all EndMT inhibitor groups did not differ significantly from each other but immature hearts exposed to myocardial strain significantly showed more endocardial endothelial cells EndMT mediated through activation of the TGF-ß pathway. These data were confirmed by staining of nuclear colocalization of the transcription factors SLUG/SNAIL (**See Figure 17**).

In all mature hearts, stretch did not induce endocardial EndMT. Stretch alone and addition of TGF-β inhibitors did not show any significant difference in the number of double-stained endocardial cells compared to unstretched controls (control: 2± 0.6, stretch: 5%± 1.2, stretch+BMP-7: 4.6%± 0.1, stretch+SB-431542: 2.1± 0.06; stretch+losartan: 1.8%± 0.5; $P>0.05$) (**Figure 18**).

These results were confirmed by staining for SLUG/SNAIL which showed equivalent result with no significant difference between the groups (67) (**Figure 19**).

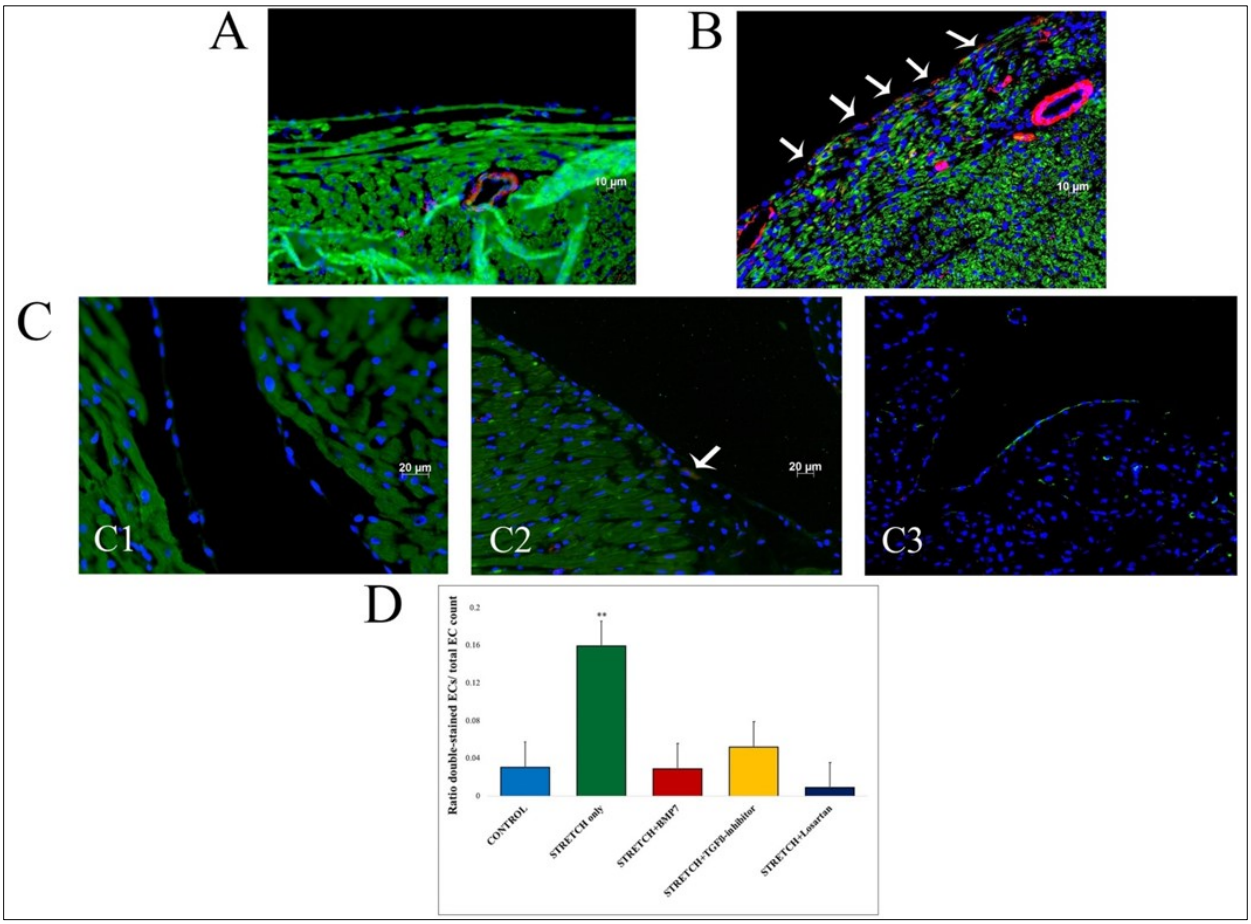

Figure 17: Immature hearts were perfused in a non-working Langendorff set-up and exposed to static uniaxial stretch with 10x their heart weight for 3 hours. Heart tissue was stained for the endothelial marker PECAM1 (green), the mesenchymal marker αSMA (red) and DAPI (blue). Double staining for both PECAM1 and αSMA indicated EndMT (white arrows point out EndMT positive ECs). Representative immunohistochemical stains for double-labelling of ECs with PECAM1 and αSMA are shown for (A) control hearts, (B) immature rat hearts stretched for 3 h , (C) immature hearts stretched with an inhibitor present (BMP-7 on the left, TGF-β-inhibitor in the middle, Losartan on the right). Panel (D) shows supporting evidence by staining for the transcription factors SLUG/SNAIL (red) which indicated active EndMT by double-staining of nuclei with DAPI in blue. (E) Summary of the results are shown in this graph. Ratio of double stained (CD31/alpha-SMA) endothelial cells/ total endothelial cell count in controls, stretched and stretch with inhbitors are shown. There were significantly more double-stained cells in stretched hearts compared to all other groups (**=$p<0.05$) but there was no significant difference between the other. (© V. WEIXLER)

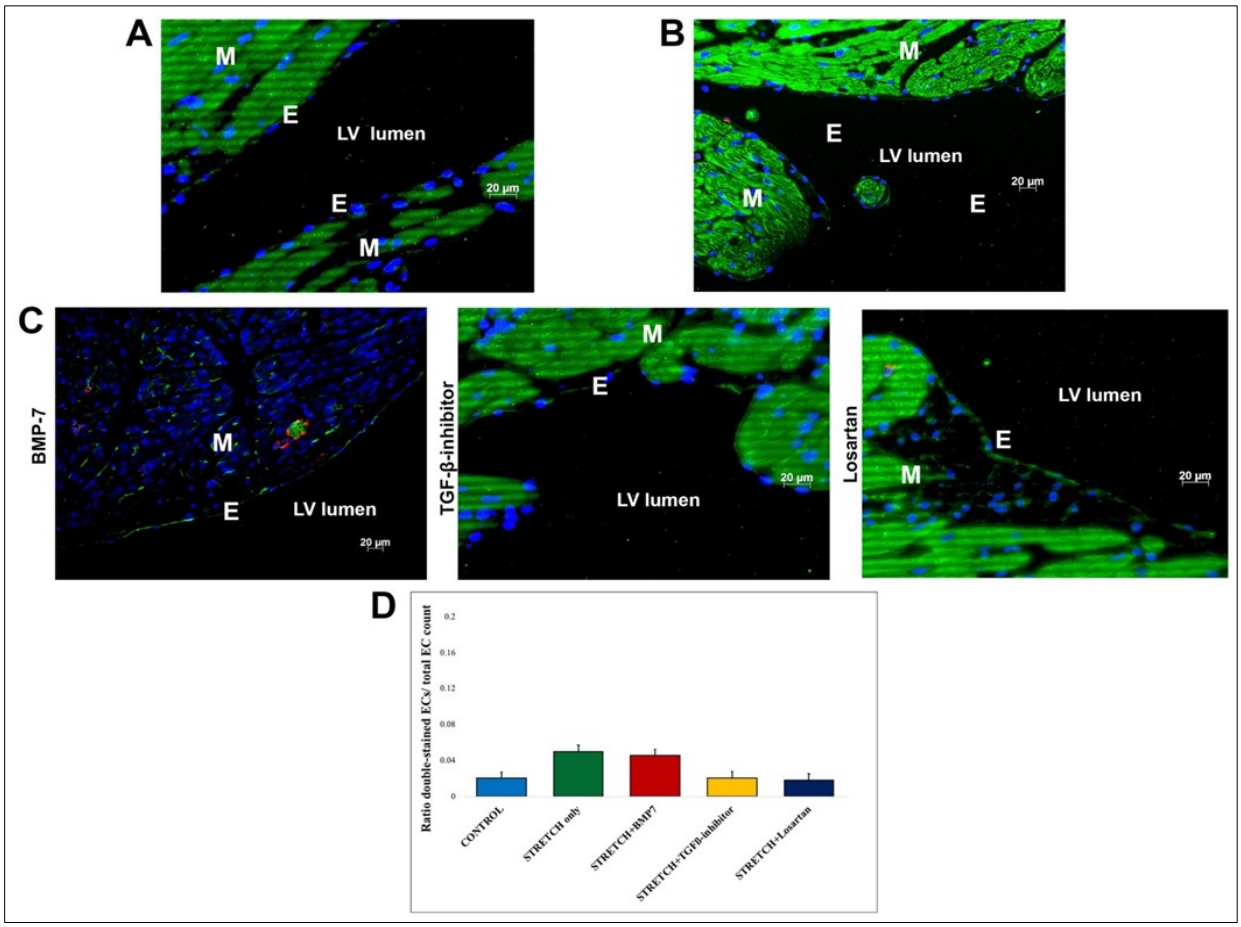

Figure 18: Mature hearts were perfused in a non-working Langendorff set-up and exposed to static uniaxial stretch with 10x their heart weight for 3 hours. Heart tissue was stained for the endothelial marker PECAM1 (green), the mesenchymal marker αSMA (red) and DAPI (blue). Double staining for both PECAM1 and αSMA indicated EndMT. Representative immunohistochemical stains for double-labelling of ECs with PECAM1 and αSMA are shown for (A) control hearts, (B) mature rat hearts stretched for 3 h, (C) mature hearts stretched with an inhibitor present (BMP-7 on the left, TGF-β-inhibitor in the middle, Losartan on the right). (D) Summary of the results are shown in this graph. Ratio of double stained (CD31/alpha-SMA) endothelial cells/ total endothelial cell count in controls, stretched and stretch with inhibitors are shown. There were no significant differences between the groups. Uniaxial stretch in mature hearts did not induce endocardial EndMT. (© V. WEIXLER)

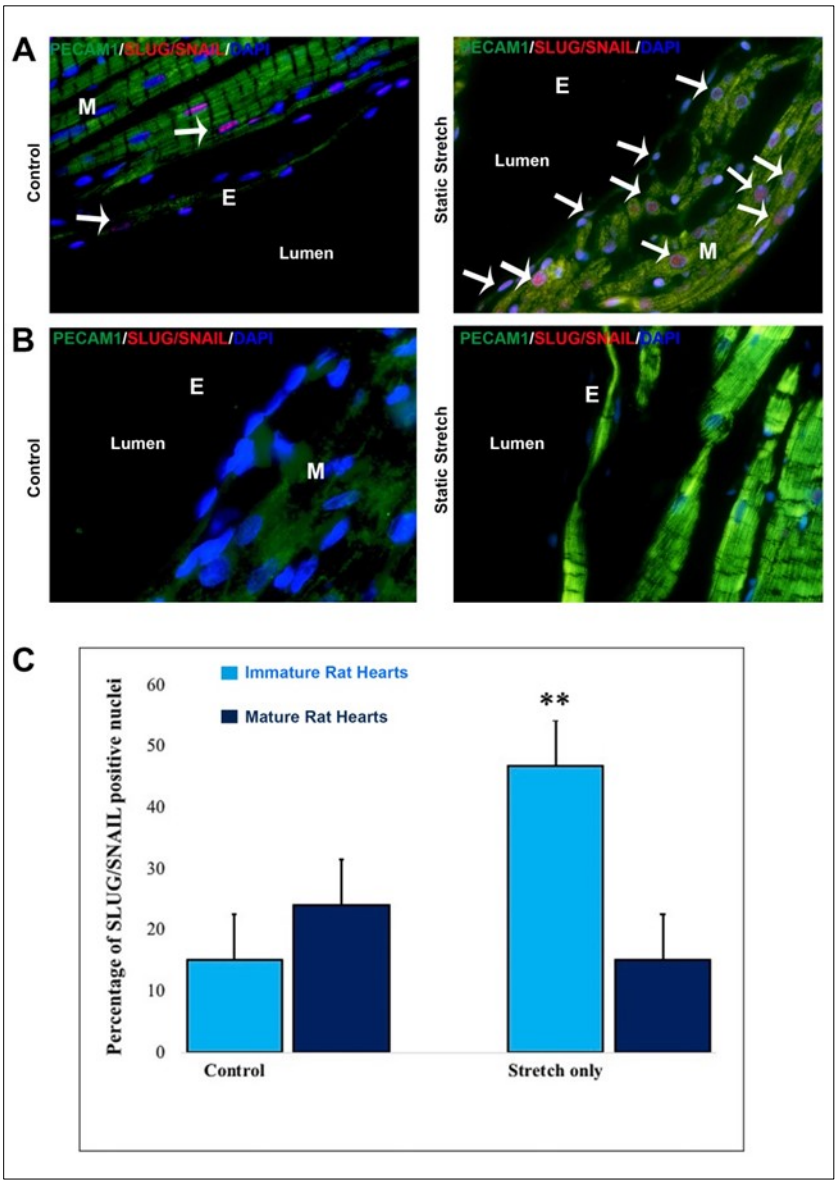

Figure 19: Immature (A) and mature hearts (B) were perfused in a non-working Langendorff set-up and exposed to static uniaxial stretch with 10x their heart weight for 3 hours. Heart tissue was stained for the endothelial marker PECAM1 (green), SLUG/SNAIL (red) and DAPI (blue). Immature hearts showed supporting evidence by staining for the transcription factors SLUG/SNAIL (red) which indicated active EndMT by double-staining of nuclei with DAPI in blue. (C) Summary of the results are shown in this graph. Ratio of double stained (SLUG/SNAIL/alpha-SMA) endothelial cells/ total endothelial cell count in controls and stretched for immature and mature hearts. There were no significant differences between the groups in the mature rat hearts. Uniaxial stretch in mature hearts did not induce endocardial EndMT. In contrast, immature rat hearts showed significantly more cells undergoing Endmt in stretched hearts compared to controls (**=$p<0.05$). (© V. WEIXLER)

3.3. Analyzing Human EFE Tissue

3.3.1. Patients

The median age of HLHS patients at the time of most recent EFE resection was 27 months (IQR=0 – 73.5 months) compared to a median age of 36 months (IQR=0.8 – 73.3 months) in the non-HLHS patient group (P=0.8).

In the consented HLHS patient group, apart from the main diagnosis of HLHS, aortic regurgitation (AR) especially following post-natal balloon valvuloplasty was described in four patients; mitral stenosis (MS) due to a dysplastic mitral annulus was found in five of seven patients. These valvar diseases caused turbulent flow within the LV in all seven consented HLHS patients, which was described throughout their entire medical history. All except for two HLHS patients had previous EFE resections. At the time of the most recent resection, all valvar diseases were successfully repaired and no remaining turbulences were described postoperatively and at follow-up neither in echocardiography nor in MRI studies. The median follow-up time after the last EFE resection in the consented HLHS patient was 6.8 months (IQR=4.15 - 9.45 months) (**Table 22**). In the "non-HLHS" patient group with valvar disease, a jet across a stenotic MV was present predominantly. In two cases, a regurgitant AV caused a jet toward the LVOT (**Table 23**) (62).

Patient	Age	Diagnosis	Performed procedures	# of EFE resections	Localization of EFE resection
1	5 y	HLHS, AS, **MS (jet caused by MV)**	**MV repair 2x, MV replacement (Melody), MV replacement (epic porcine valve)**	**5** (2013, 2014, 2015, 2017)	LV, septum, papillary muscles
2	2 y	HLHS, MS, **AR (jet caused by AV)**	PA banding, Norwood I, Glenn, **MV/AV repair**	**1** (2017)	papillary muscles, post. LV free wall, septum
3	12 y	HLHS, AR, MR/**MS** (**jet against anterior mitral leaflet**)	PA banding, **AV/MV repair**, BT shunt, Glenn, LT Fontan	**4** (2005, 2006, 2007, 2017)	septum, below aortic valve, apex, mitral valve annulus, LA (left pulmonary vein orifice)
4	5 mo	HLHS, critical AS, **MS** (**2 small jets of inflow)**	**fetal balloon dilation,** postnatal balloon dilatation, Sano I, **AV/MV repair**, Glenn	**1** (2017)	LV free wall, papillary muscles, apex, LVOT
5	10 y	HLHS, **AR (central jet)**	**postnatal balloon dilatation**, Norwood I, BT shunt, **AV/MV repair, AV replacement**	**2** (2010, 2017)	septum, free LV wall, papillary muscles
6	9 y	HLHS, **AR (broad jet)**, MS	**postnatal balloon dilation, AV repair 2x, MV repair 2x**	**3** (2010, 2013, 2017)	posterior LV wall, septum, apex, sub-aortic region
7	7y	HLHS, **severe AR (jet anterior posterior)**	**multiple postnatal balloon dilatations**, **AV repair 2x**	**2** (2011, 2017)	Subaortic region, LVOT, septal myectomy

Note: Patient 1-7, age in years (y) or months (mo), diagnosis at time of surgery (cause of jet in bold): Hypoplastic Left Heart Syndrome (HLHS), mitral stenosis (MS), mitral regurgitation (MR), aortic stenosis (AS), aortic regurgitation (AR), aortic valve (AV), mitral valve (MV), performed procedures (cause of jet in bold): pulmonary artery (PA) banding, Blalock Taussig Shunt (BT shunt), lateral tunnel Fontan (LT Fontan), number of EFE resections (#), year of resections in brackets, localization of EFE resection: left ventricle (LV), left ventricle outflow tract (LVOT), bold

Table 22: Detailed information of consented Hypoplastic Left Heart Syndrome (HLHS) patients. Consented HLHS patients 1 – 7 are presented including age, performed surgeries in chronological order, number of EFE resections and localization of EFE tissue obtained for histological analysis, reproduced from Weixler et al. (September, 2019) with permission of Elsevier.

Patient	Age	Diagnosis	Localization of EFE resection
1	3 y	**MS (parachute valve)**	LV, supra-mitral membrane
2	3 y	**MS (jet),** AS**, fetal balloon valvuloplasty** (31 3/7 weeks)	LV, subaortic region
3	12 y	**MS** (**3 jets**)	LV (posterior MV leaflet)
4	3 mo	Shone complex, **MS (posteriorly and laterally oriented jet**), bicuspid AV	LV, papillary septal muscle
5	3 y	**MS (jet posteriorly)**	LV, mitral valve muscle
6	8 y	**AR (central jet), postnatal balloon valvuloplasty**	LV, posterior, septum

Note: Patients 1-6, age in years (y) or months (mo), diagnosis at time of surgery (cause of jet in bold): mitral stenosis (MS), mitral regurgitation (MR), aortic stenosis (AS), aortic regurgitation (AR), localization of EFE resection: left ventricle (LV).

Table 23: Detailed information of non-Hypoplastic Left Heart Syndrome (HLHS) patients. In this group of non-HLHS patients, flow disturbances in the left ventricle (LV) caused by either mitral valve stenosis (MS) or aortic valve regurgitation (AR) were in part the reason for surgical intervention. However, imaging studies did not describe any endocardial abnormalities in the sense of EFE prior to surgery. EFE resection was performed following the cardiac surgeon's ad hoc decision intraoperatively. Non-HLHS patients are presented including age, diagnosis and localization of EFE resection, reproduced from Weixler et al. (September, 2019) with permission of Elsevier.

3.3.2. Presence of EndMT:

Endocardial double-staining with CD31/alpha-SMA as well as Twist and Slug/Snail-positive stained nuclei, respectively, both indicative of active EndMT, were found not only in all of the 24 samples from HLHS patients but also in all six non-HLHS patients. EndMT-positive tissue was not found, however, in right ventricular tissue samples nor in a healthy rat heart (**Figure 20**) (62).

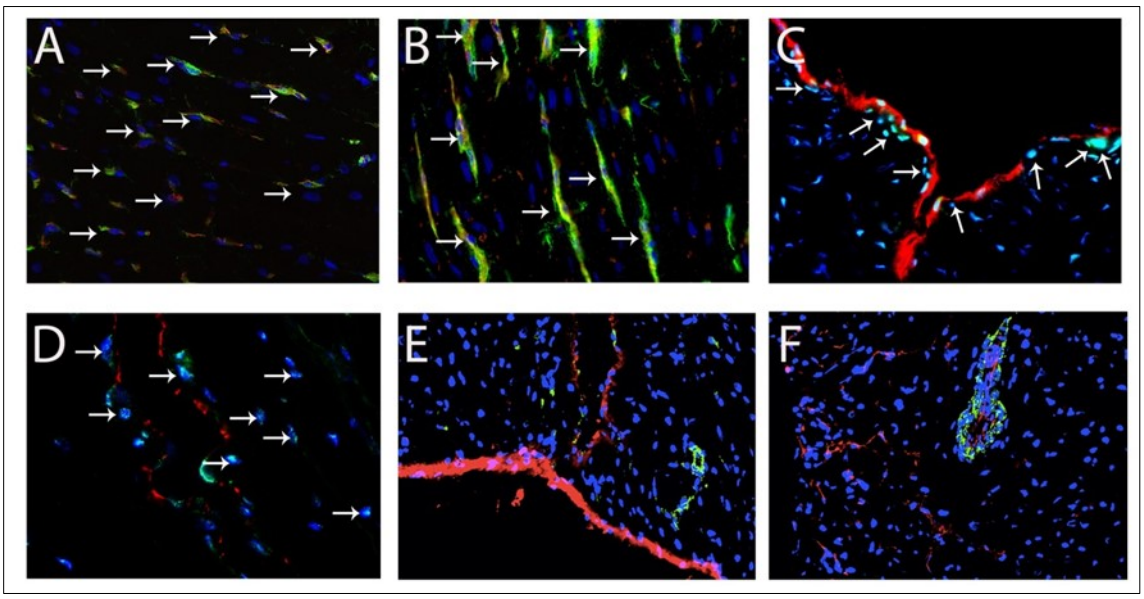

Figure 20: Representative sections of EFE and "EFE-like" tissues are displayed. Double-staining of endothelial cells with CD-31 (red) and αSMA (green), or endothelial cells with CD-31 (red) and nuclei-positive staining for transcription factors Twist and Slug/Snail (green) is indicative of active EndMT. Nuclei are stained in blue with DAPI. (A) EFE tissue from HLHS patients is positive for EndMT (CD-31/αSMA double-staining, white arrows), (B) "EFE-like" tissue from non-HLHS patients is positive for EndMT (CD-31/αSMA double-staining, white arrows). (C) EFE tissue and "EFE-like" tissue stained for the transcription factors Twist (white arrow (D) and Slug/Snail (white arrows), respectively, which are indicative of active EndMT when co-localized with endothelial cell nuclei. (E) Normal rat heart tissue and (F) human RV tissue are negative for EndMT, reproduced from Weixler et al. (September, 2019) with permission of Elsevier.

3.3.3. Composition of EFE tissue:

The number of nuclei (mean±SEM expressed as nuclei per field of vision) within EFE tissue decreased with increasing age – infants (<1 year of age) 282±63 versus toddlers and pre-schoolers (1-5 years of age) 158±24 versus school-aged children (>5 years of age with the oldest child at 12 years of age) 94±12 but did not reach significance. All tissue remained avascular in all tissue samples. EFE tissue from HLHS patients consisted predominantly of elastic and collagen fibres with some underlying myocardium. The ratio of muscle to elastin and collagen did not show any age-related trend (**Figure 21**). "EFE-like" tissue obtained from non-HLHS patients, showed the same characteristics as EFE tissue from HLHS patients. Collagen and elastin predominated the tissue sections, the number of nuclei decreased with age, and there were no blood vessels found within the tissue(62).

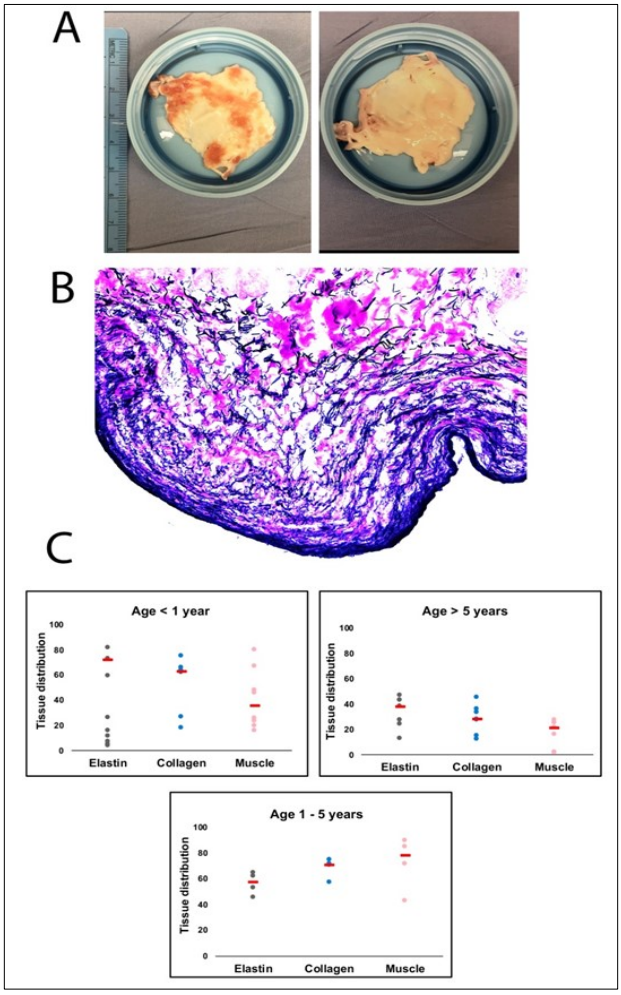

Figure 21: (A) Macroscopic appearance of resected EFE tissue from left ventricle (LV) of Hypoplastic Left Heart Syndrome (HLHS) patient, left: tissue sample facing towards the myocardium (red=muscle), right: sample side facing towards ventricular lumen. (B) Van Giesson Elastin (VG) stain of a representative picture showing the distribution of collagen (blue), elastin (black) and muscle (white-yellow) in EFE tissue samples. (C) Distribution of elastin, collagen and muscle within specific age groups (<1 year, 1-5 years, > 5 years), dot plot charts showing all values plotted in different colors (collagen=blue, elastin=black, muscle=pink), medians of each column shown as red bar, reproduced from Weixler et al. (September, 2019) with permission of Elsevier.

3.3.4. Analysis of Myocardium:

In all patients with EFE and "EFE-like" tissue, some underlying myocardium was resected. MT stains showed infiltrative growth of collagen bundles from the endocardium into the underlying

myocardium of HLHS patients and non-HLHS patients with flow disturbances. The degree of infiltrative growth increased with increasing age. In samples of patients <1 year of age, the fibrotic tissue was separated from the underlying muscle, whereas in samples from older children (> 2years of age), no separation between collagen fibers and myocardium was feasible and collagen grows more infiltrative (**Figure 22**)(63). Also in patients, in which EFE was resected multiple times, EFE bundles started growing more infiltrative into the underlying myocardium (**Figure 23**). The endocardial thickness of fibrotic tissue decreases, whereas infiltrative growth of collagen into the underlying myocardium increases. In contrast, in a healthy rat heart and RV tissue samples, a thin endocardial layer is present which is separated from the underlying myocardium (**Figure 24**) (63). Localization of endothelial cells within the collagen-rich tissue which infiltrates the myocardium identified multiple double-stained cell for CD31 and alpha-SMA. The double-staining is indicative that intramyocardial fibrotic tissue is also derived through EndMT (**Figure 25**) (62,63).

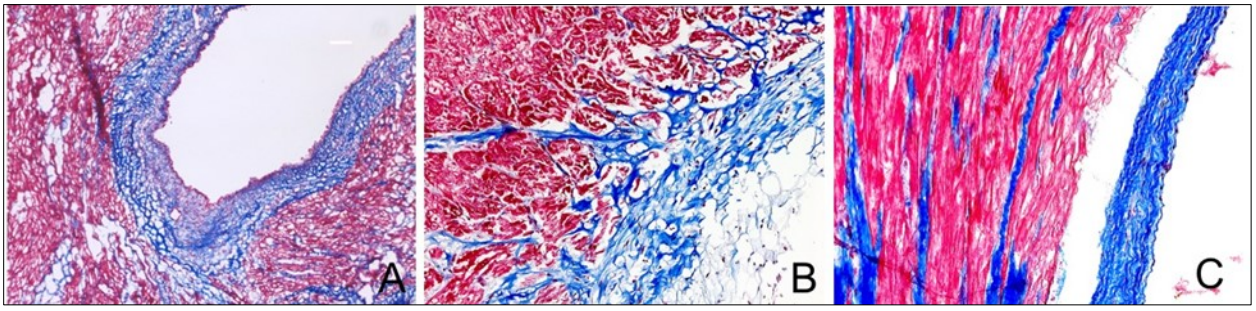

Figure 22: Increasing degree of infiltrative growth of EFE tissue with increasing of age, MT stains (collagen=blue, underlying muscle=red) showing different aged samples: (A) 10-day old newborn, (B) 2-year old child, (C) 11-year old child, reproduced from Weixler et al. (September, 2019) with permission of Elsevier.

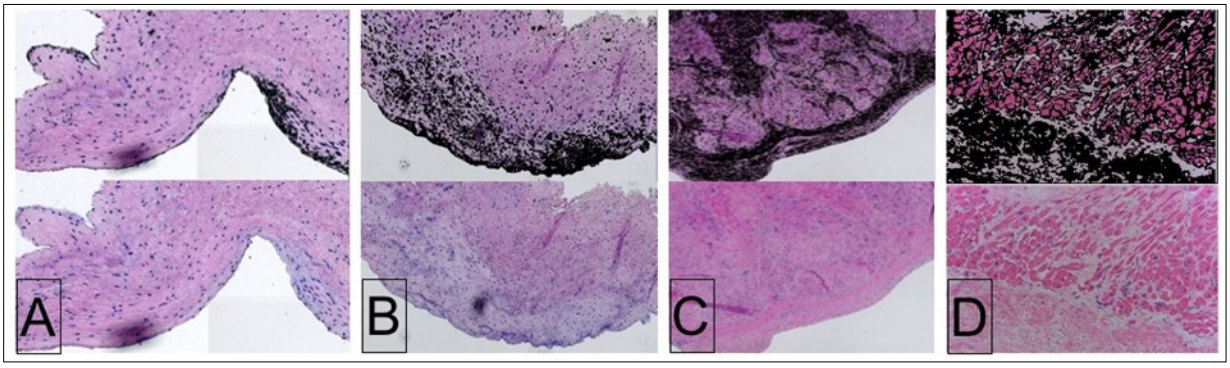

Figure 23: HE stains from 4 different resection (1rst, 2nd , 4th , 6th), ordered from A-D. Left picture: original HE stain (collagen in light pink/blue, muscle in red), Right picture: Collagen marked in black; with each resection collagen is growing infiltrative into the underlying myocardium, reproduced from Weixler et al. (April, 2019) with permission of Elsevier.

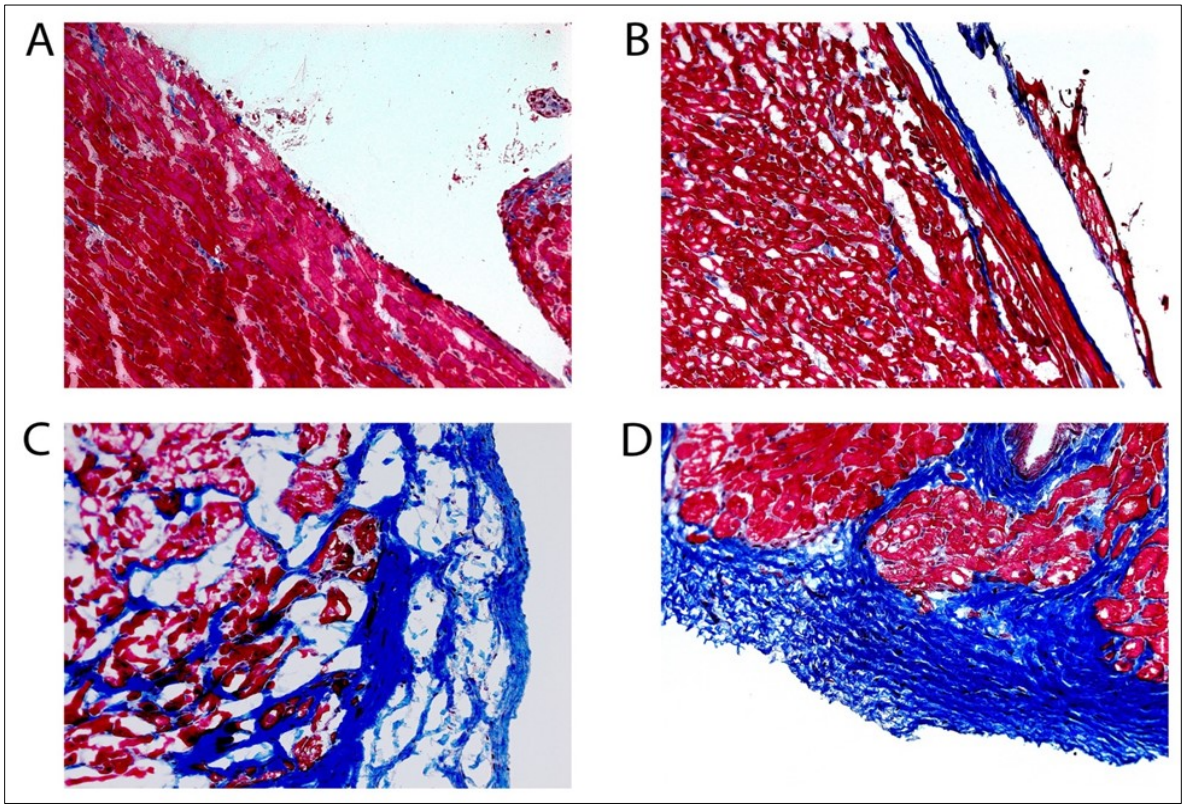

Figure 24: Distribution of collagen and muscle tissue on Masson's Trichrome stains is shown for a (A) normal rat heart, (B) normal human tissue, (C) LV of HLHS-patient, and (D) LV of non-HLHS patient. Muscle is stained in red and collagen in blue where if the latter is not limited to the endocardial surface but grows infiltratively into the underlying myocardium in (C) and (D), reproduced from Weixler et al. (September 2019) with permission of Elsevier.

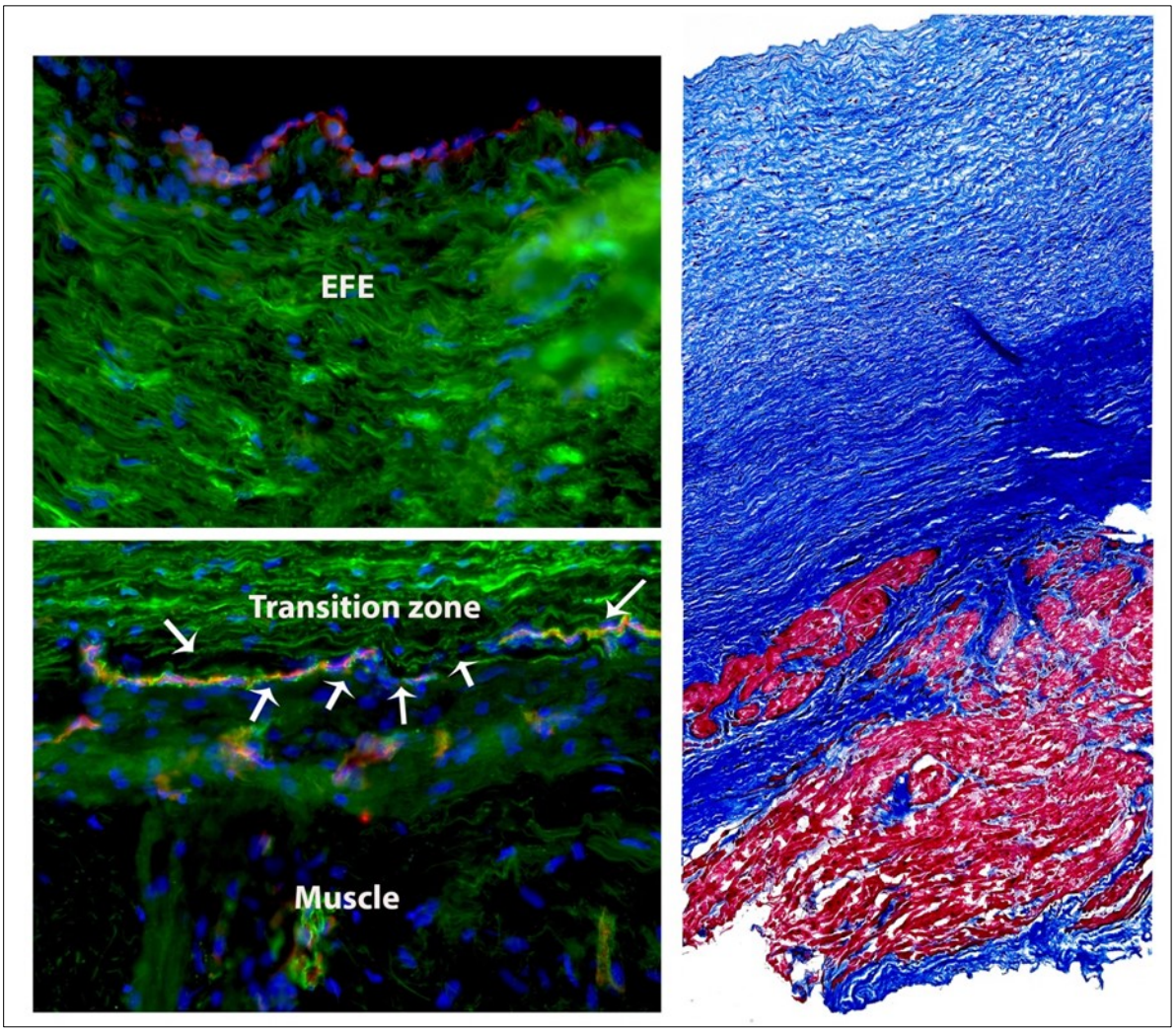

Figure 25: EFE tissue that infiltrates the myocardium stains positive for EndMT. A representative section of EFE tissue was stained with Masson's Trichrome (blue: collagen fibers, red: myocardium) and correspondingly on the left, the same areas were stained to identify active EndMT (green: α-SMA, red: CD31, blue: DAPI). Double-staining is indicative for EndMT (white arrows) which is more pronounced in the transition zone between endocardial thickening due to EFE tissue and the underlying myocardium, reproduced from Weixler et al. (September, 2019) with permission of Elsevier.

3.3.5. Elastase/Matrix Metalloproteinase activity:

In situ zymography displayed a balance between degradation of elastin and collagen and elastase/gelatinase activity in each individual sample but no age-related trend could be identified (**Figure 26**). The same characteristics were found in the non-HLHS patients with flow disturbances (62).

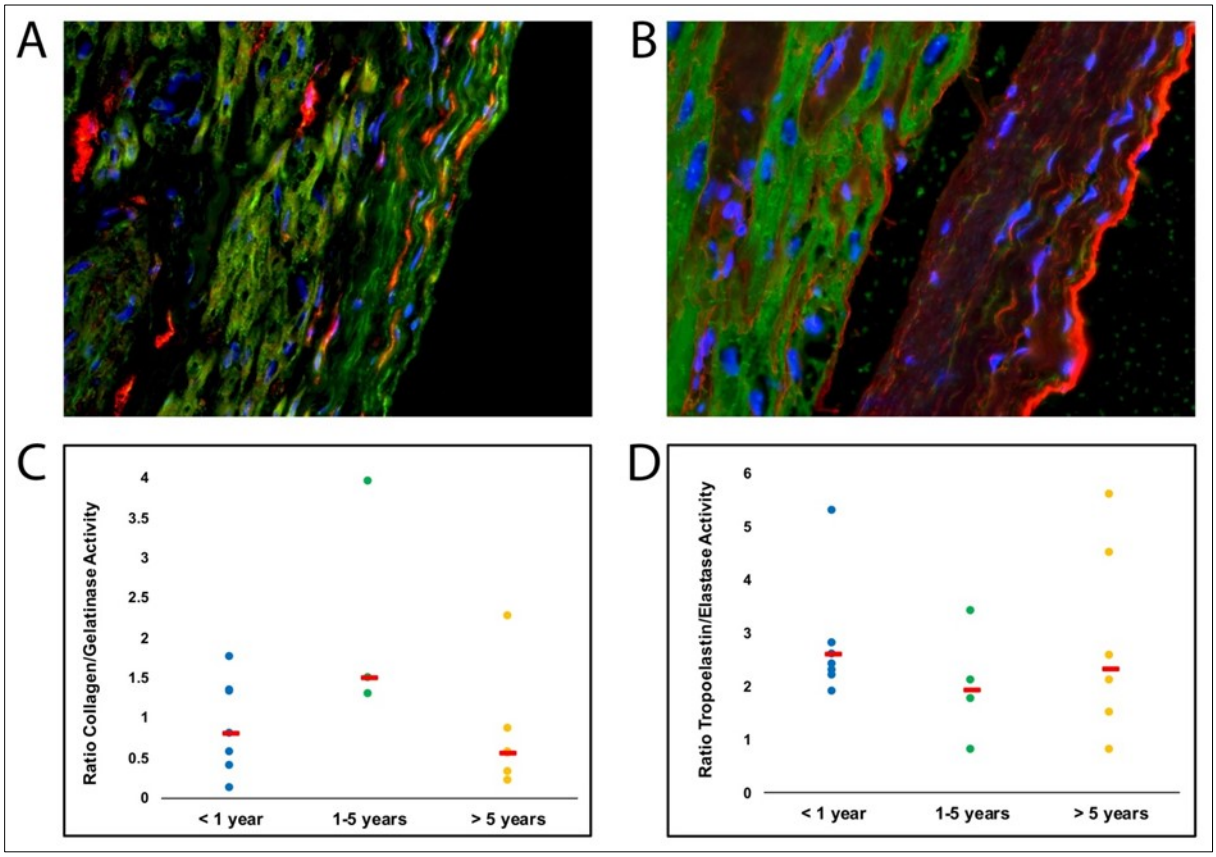

Figure 26: In situ zymography of gelatinase activity and collagen/elastase activity and tropoelastin
(A) Representative in situ zymography of gelatinase activity and collagen in EFE tissue obtained from HLHS patients is shown. Gelatinase is shown in green, collagen in red and nuclei (DAPI) in blue.(B) Representative in situ zymography of elastase activity and tropoelastin in EFE tissue obtained from HLHS patients is shown. Elastase is shown in green, tropoelastin in red and nuclei (DAPI) in blue. (C and D) Summary of MMP activity (gelatinase on the left and elastase on the right) per field of vision is shown using dot plot charts showing all values plotted for different age groups (<1 year, 1-5 years, > 5 years), medians of each column shown as red bar. There was no significant age-related difference in the balance of MMP activity to collagen/elastin production, reproduced from Weixler et al. (September, 2019) with permission of Elsevier.

4. Discussion

By conducting this thesis, I was able to show that EndMT, induced by TGF-ß and inhibited by blocking the TGF-ß pathway, is a process not only limited to the symptom complex of HLHS. Mechanical stimuli such as hemodynamic alterations like strain and flow disturbances were the triggers for EndMT induction. Despite the fact that initial EFE development through activation of EndMT was shown to be an age-dependent process, progression of EFE continues throughout childhood but changes its appearance from restricted to the endocardium to myocardial infiltrative growth (62,63). In the cell culture experiments of this study, EndMT was successfully induced by exposing ECs to uniaxial stretch and was inhibited by adding BMP-7 or direct TGF-ß-inhibitors to the media. These results corresponded with the *ex vivo* whole heart preparation, in which I demonstrated that endocardial fibrosis is an age-dependent process which results as a consequence of increased strain on the left ventricle and that increased mechanical forces mediate activation of the TGF-β pathway leading to EndMT of endocardial endothelial cells. Rebalancing the TGF-β/BMP pathway through addition of BMP-7, or direct inhibition of TGF-β, or clinically relevant localized application of Losartan at the site of fibrosis, respectively, showed significant reduction in EndMT of endocardial endothelial cells (67).

ECs contribute to pathological processes such as organ fibrosis through a process called EndMT where ECs transform to mesenchymal cells. Furthermore, in cancer pathology it has been shown that cells achieve the ability to migrate and transform into malignant cells via EndMT (68). EndMT has been identified as a new therapeutic target for fibrotic disorders such as pulmonary, intestinal, cardiac and kidney fibrosis (32,69,70). EndMT is regulated mainly through activation of TGF-β but the exact stimuli for TGF-β activation under physiologic and/or pathologic conditions are still under investigation.

Unlike myocardial fibrosis in hypertrophy and heart failure, endocardial fibrosis is predominantly present in young, immature hearts and originates from the endocardium as we have recently reported (31,54). Furthermore, an imbalance of the BMP/TGF-β pathway due to hypermethylation of the BMP7 promoter was identified as trigger for TGF-β mediated EndMT (31). Clinical observation indicates that hemodynamic alterations imposed on the growing heart likely stimulate EndMT of endocardial endothelial cells and mechanical strain such as distention of the LV negatively impacts progression of this fibrotic process especially in utero. ECs are stabilized by their environment and respond to mechanical forces by changing their behavior. In isolated human umbilical vein endothelial cells, it has already been reported that cyclic stretch induces EndMT through an integrin β1 pathway (71).

To further investigate mechanical triggers for EndMT activation while controlling for flow, an in vitro cell culture model was developed. HCAEC were used since they are known for overlapping embryogenic origin as endocardial cells (57). Cells were exposed to uniaxial static stretch inducing EndMT which was confirmed by immunohistochemical assessment of double-stained cells (72). These results suggested that mechanical forces can lead to phenotypical changes of ECs.

Isolated cells in culture have limitations due to lack of interaction with other myocardial cells. Thus, I used whole a whole heart preparation to confirm these cell culture findings of inducing EndMT through stretch. Isolated mechanical strain without exposure of the endocardium to flow was also achieved in this whole heart preparation. I was able to show that endocardial cells underwent EndMT when exposed to mechanical strain. However, only immature hearts responded by induction of EndMT suggesting an age-related component to the development of endocardial fibrosis.

To determine whether the TGF-ß pathway was involved in the regulation of stretch-induced EndMT, I exposed stretched endothelial cells and stretched hearts to local inhibitors of the TGF-ß pathway. The choice of inhibitors used in this study was based on our previous data where my research group unraveled an imbalance of the TGF-ß/BMP-7 pathway in EndMT-induced fibrosis of the endocardium. Secondly, I used a specific TGF-ß inhibitor that directly blocks TGF-ß binding to the ALK 5 kinase receptor. Furthermore, from a clinical perspective, my goal was to identify a clinically applicable inhibitor and thus, I tested Losartan which as an Angiotensin receptor inhibitor blocks the TGF-ß pathway indirectly (56).

The control and all EndMT inhibitor groups did not differ significantly from each other but immature hearts exposed to myocardial strain significantly showed more endocardial endothelial cells undergoing EndMT mediated through activation of the TGF-β pathway (67). BMP7 has already been shown to inhibit EndMT *in vitro* in cell culture and *in vivo* in a rat model of endocardial fibroelastosis which we confirmed in this whole heart preparation (31).

The ALK5 kinase inhibitor SB-431542 has previously been shown to upregulate claudin-5, a component of the endothelial tight junction responsible for cell-cell contacts in cell culture (55). Confirmation of TGF-β's main regulatory role in endocardial fibrosis development in immature hearts, was supported by staining for the transcription factors SLUG/SNAIL which are downstream of TGF-ß-regulated expression of VE-cadherin. Immature hearts exposed to myocardial strain had significantly more nuclei staining positive for SLUG/SNAIL corresponding to the number of double-stained endocardial endothelial cells with endothelial markers (VE-cadherin, PECAM1) and mesenchymal markers (α-SMA) (73).

This data show for the first time that only immature hearts exposed to increased myocardial strain develop endocardial endothelial changes but mature hearts do not at least in the short time frame

of exposure to increased strain. These experimental data fit well with clinical observation that endocardial EndMT is a disease affecting young patients and transforms into a more invasive growth pattern affecting the underlying myocardium with increasing age displaying the histological picture of myocardial fibrosis of adult heart failure.

Analyzing human EFE tissue, I established that structural changes of EFE tissue toward a more infiltrative growth into the underlying myocardium and less cellularity occurs with increasing age which is accompanied by decreased diastolic compliance of the ventricle (63). Furthermore, I was able to describe for the first time that hemodynamic alterations in the way of jets on the level of the mitral valve or regurgitant flow across an incompetent aortic valve promote localized aggravated EFE growth and reoccurrence despite excessive surgical resection. “EFE-like” tissue growth independent of an underlying HLHS diagnosis, shows the same pattern (62). Following detailed analysis of this “EFE-like” tissue, I determined that the underlying mechanism for development is EndMT which we had already reported in detail in patients with EFE associated with HLHS (31,62). This data further indicates that HLHS alone does not predispose this patient cohort to EFE formation but that the underlying communality is the presence of valvar defects represented as either mitral stenosis or aortic insufficiency. Both valvar defects result in flow disturbances, displayed as jets across the valve onto localized areas of the LV cavity which responds by endocardial thickening through subendocardial development of EFE tissue. In HLHS patients, despite several surgical resections of this tissue, progression still occurs unless the valvar defect is repaired (62).

Another novel finding of this study is that unlike previously suggested, EFE develops and progresses as a distinct layer of fibrotic tissue which can be easily dissected from the underlying myocardium (29). Following thorough examination of our resected tissue samples from HLHS and

non-HLHS patients, all EFE tissue samples contained some degree of muscle tissue. Macroscopically this finding suggests infiltrative growth of EFE tissue into the underlying myocardium which we confirm microscopically through MT staining. With increasing age, subendocardial tissue growth takes on a more infiltrative pattern with collagen and elastin bundles protruding into the adjacent myocardium. This change in growth pattern in HLHS patients is reflected by an elevated end-diastolic pressure but growth of the once diminutive LV is maintained indicated by increasing end-diastolic volumes (62,63). Thus, the current data show that the main trigger for the development and progression of EFE is flow disturbances, which might also occur in other congenital heart diseases leading to macroscopically "EFE-like" tissue unrelated to the primary diagnosis of HLHS.

In the EFE tissue samples, we could show that localized response of the endocardium to flow disturbances (e.g. shear stress) created EFE (62). It is well known that endothelial cells lining the vasculature respond to alterations in shear stress by changing their shape and function (74) since they are exposed to a large variety of biochemical and hemodynamic stimuli. Thus, endothelial cells are required to be highly plastic which allows for adaptation to alterations in fluid shear forces. Plasticity is essential to maintain homeostasis but pathological stimuli might alter this process and contribute to disease through adverse plasticity which EndMT is an example of (37). Areas exposed to disturbed blood flow and thus, alterations in shear stress generate a microenvironment conducive for EndMT. As a consequence, activation of EndMT results in intimal hyperplasia with extracellular matrix remodeling (37,75). EFE has the appearance of organized layers resembling degenerative intimal hyperplasia of arterial vessel walls. The details on hemodynamic forces and their role in maintaining vascular integrity have been well studied in the vasculature but little is known whether laminar shear stress is protective also for the

endocardial endothelial cells. The preliminary data I obtained from the in vitro flow chamber experiments showed that ECs undergo EndMT with turbulent but not laminar flow, which certainly needs to be confirmed in further experiments. However, it supports the idea that flow disturbances may play a role in endocardial remodeling through EndMT driven by activation of transcription factors which are actively involved in suppression of VE-cadherins and other endothelial specific proteins. Furthermore, in an animal model of EFE formation which we had previously described in detail, an association with alterations in mechanical forces including flow disturbances across an incompetent aortic valve is associated with formation of EFE (39,62).

Functional indicators of EndMT in tissue are increased expression of collagens and elastin, as well as production of enzymes degrading the extracellular matrix, such as matrix metalloproteinase-2 (MMP)-2, MMP-9 or MMP-12 (elastase). The expression of mesenchymal markers corresponds to a newly acquired ability to produce and remodel the extracellular matrix (62,76). With regard to remodeling, activation of MMPs are important following the interruption of cell-cell or cell-matrix contact. In the present patient cohort, no defect in the degradative potential of the extracellular matrix of the endocardium or myocardium was found since all MMPs (MMP12 and MMP2/9) were active in all tissue samples but distribution was focused on areas of active remodeling (62,63).

In summary, with this work I could successfully demonstrate that EndMT induction is triggered by different mechanical forces such as strain and flow on the endocardium. By use of specific inhibitors, I could show that this endocardial fibrotic process is TGF-ß pathway mediated and clinically relevant drugs such as BMP-7 and Losartan successfully inhibited this process preserving the endocardium. Immaturity plays an important role in the development of EFE,

nevertheless the progression doesn’t stop as the patient grows older, but much more takes on a more infiltrative pattern when trigger is not eliminated (63).

5. References

1. Hickey EJ, Caldarone CA, McCrindle BW. Left ventricular hypoplasia: A spectrum of disease involving the left ventricular outflow tract, aortic valve, and aorta. J Am Coll Cardiol. 2012;

2. Murdison KA, Baffa JM, Farrell PE, Chang AC, Barber G, Norwood WI, et al. Hypoplastic left heart syndrome. Outcome after initial reconstruction and before modified Fontan procedure. Circulation. 1990;82(5 Suppl):IV199-207.

3. Parker SE, Mai CT, Canfield MA, Rickard R, Wang Y, Meyer RE, et al. Updated national birth prevalence estimates for selected birth defects in the United States, 2004-2006. Birt Defects Res A Clin Mol Teratol. 2010 Dec;88(12):1008–16.

4. Barron DJ, Kilby MD, Davies B, Wright JGC, Jones TJ, Brawn WJ. Hypoplastic left heart syndrome. Lancet. 2009;374(9689):551–64.

5. Olley PM, Coceani F, Bodach EVA. E-Type Prostaglandins Congenital Heart Malformations. Circulation. 1976;728–31.

6. Akintuerk H, Michel-Behnke I, Valeske K, Mueller M, Thul J, Bauer J, et al. Stenting of the arterial duct and banding of the pulmonary arteries: Basis for combined Norwood stage I and II repair in hypoplastic left heart. Circulation. 2002;

7. Sharland GK, Allan LD. Screening for congenital heart disease prenatally. Results of a 21/2-year study in the South East Thames Region. BJOG Int J Obstet Gynaecol. 1992 Mar;99(3):220–5.

8. Allan LD, Sharland GK, Milburn A, Lockhart SM, Groves AM, Anderson RH, et al. Prospective diagnosis of 1,006 consecutive cases of congenital heart disease in the fetus. J Am Coll Cardiol. 1994 May;23(6):1452–8.

9. McElhinney DB, Marshall AC, Wilkins-Haug LE, Brown DW, Benson CB, Silva V, et al. Predictors of technical success and postnatal biventricular outcome after in utero aortic valvuloplasty for aortic stenosis with evolving hypoplastic left heart syndrome. Circulation. 2009 Oct 13;120(15):1482–90.

10. McElhinney DB, Tworetzky W, Lock JE. Current Status of Fetal Cardiac Intervention. Circulation. 2010 Mar 16;121(10):1256–63.

11. Maxwell D, Allan L, Tynan MJ. Balloon dilatation of the aortic valve in the fetus: a report of two cases. Br Heart J. 1991 May;65(5):256–8.

12. Freud LR, McElhinney DB, Marshall AC, Marx GR, Friedman KG, del Nido PJ, et al. Fetal Aortic Valvuloplasty for Evolving Hypoplastic Left Heart Syndrome: Postnatal Outcomes of the First 100 Patients. Circulation. 2014 Aug 19;130(8):638–45.

13. Sharland GK, Chita SK, Fagg NLK, Anderson RH, Tynan M, Cook AC, et al. Left ventricular dysfunction in the fetus : relation to aortic valve anomalies and endocardial fibroelastosis.

14. McElhinney DB, Vogel M, Benson CB, Marshall AC, Wilkins-Haug LE, Silva V, et al. Assessment of Left Ventricular Endocardial Fibroelastosis in Fetuses With Aortic Stenosis and Evolving Hypoplastic Left Heart Syndrome. Am J Cardiol. 2010 Dec;106(12):1792–7.

15. Emani SM, Bacha EA, McElhinney DB, Marx GR, Tworetzky W, Pigula FA, et al. Primary left ventricular rehabilitation is effective in maintaining two-ventricle physiology in the borderline left heart. J Thorac Cardiovasc Surg. 2009 Dec;138(6):1276–82.

16. Norwood W, Lang P, Hansen D. Physiologic Repair of Aortic Atresia-Hypoplastic Left Heart Syndrome. N Engl J Med. 1983;308.

17. Norwood W, Kirklin JK, Sanders SP. Hypoplastic Left Heart Syndrome : Experience With Palliative Surgery. 1990;45(January):87–91.

18. Schmid C, Asfour B. Leitfaden Kinderherzchirurgie. Heidelberg: Steinkopff; 2009.

19. Khairy P, Fernandes SM, Mayer JE, Triedman JK, Walsh EP, Lock JE, et al. Long-Term Survival, Modes of Death, and Predictors of Mortality in Patients With Fontan Surgery. Circulation. 2008 Jan;117(1):85–92.

20. Herrin MA, Zurakowski D, Baird CW, Banka P, Esch JJ, del Nido PJ, et al. Hemodynamic parameters predict adverse outcomes following biventricular conversion with single-ventricle palliation takedown. J Thorac Cardiovasc Surg. 2017;

21. Kantrowitz A, Haller JD, Joos H, Cerruti MM, Carstensen HE. Transplantation of the heart in an infant and an adult. Am J Cardiol. 1968 Dec;22(6):782–90.

22. Moons P, Bovijn L, Budts W, Belmans A, Gewillig M. Temporal Trends in Survival to Adulthood Among Patients Born With Congenital Heart Disease From 1970 to 1992 in Belgium. Circulation. 2010 Nov 30;122(22):2264–72.

23. Bailey LL. The Evolution of Infant Heart Transplantation. J Heart Lung Transplant. 2009;28(12):1241–5.

24. Dipchand AI, Kirk R, Edwards LB, Kucheryavaya AY, Aurora P, Christie JD, et al. The Registry of the International Society for Heart and Lung Transplantation: thirteenth official pediatric heart transplantation report--2010. J Heart Lung Transplant. 2010;29(10):1119–28.

25. Chinnock RE, Bailey LL. Heart transplantation for congenital heart disease in the first year of life. Curr Cardiol Rev. 2011;7(2):72–84.

26. Weinberg T, Himmelfarb A. Endocardial fibroelastosis (so-called fetal endocarditis). A report of two cases occuring in siblings. Bull Johns Hopkins Hosp. 1943 Nov;26(5):299.

27. Dincsoy MY, Dincsoy HP, Kessler AD, Jackson MA, Sidbury JB. Generalized glycogenosis and associated endocardial fibroelastosis. J Pediatr. 1965 Nov;67(5):728–40.

28. Nield LE, Smallhorn JF, Benson LN, Hornberger LK, Silverman ED, Taylor GP, et al. Endocardial fibroelastosis associated with maternal anti-Ro and anti-La antibodies in the absence of atrioventricular block. J Am Coll Cardiol. 2002 Aug;40(4):796–802.

29. Emani SM, McElhinney DB, Tworetzky W, Myers PO, Schroeder B, Zurakowski D, et al. Staged Left Ventricular Recruitment After Single-Ventricle Palliation in Patients With Borderline Left Heart Hypoplasia. J Am Coll Cardiol. 2012 Nov;60(19):1966–74.

30. Eisenberg LM, Markwald RR. Molecular Regulation of Atrioventricular Valvuloseptal Morphogenesis. Circ Res. 1995 Jul 1;77(1):1–6.

31. Xu X, Friehs I, Hu TZ, Melnychenko I, Tampe B, Alnour F, et al. Endocardial fibroelastosis is caused by aberrant endothelial to mesenchymal transition. Circ Res. 2015;116(5):857–66.

32. Zeisberg EM, Tarnavski O, Zeisberg M, Dorfman AL, McMullen JR, Gustafsson E, et al. Endothelial-to-mesenchymal transition contributes to cardiac fibrosis. Nat Med. 2007 Sep 29;13(8):952–61.

33. Potenta S, Zeisberg E, Kalluri R. The role of endothelial-to-mesenchymal transition in cancer progression. Br J Cancer. 2008;99(9):1375–9.

34. Zeisberg EM, Potenta S, Xie L, Zeisberg M, Kalluri R. Discovery of Endothelial to Mesenchymal Transition as a Source for Carcinoma-Associated Fibroblasts. Cancer Res. 2007 Nov 1;67(21):10123–8.

35. Markwald RR, Fitzharris TP, Smith WNA. Structural analysis of endocardial cytodifferentiation. Dev Biol. 1975 Jan;42(1):160–80.

36. Medici D, Kalluri R. Endothelial–mesenchymal transition and its contribution to the emergence of stem cell phenotype. Semin Cancer Biol. 2012 Oct;22(5–6):379–84.

37. Moonen JRAJ, Lee ES, Schmidt M, Maleszewska M, Koerts JA, Brouwer LA, et al. Endothelial-to-mesenchymal transition contributes to fibro-proliferative vascular disease and is modulated by fluid shear stress. Cardiovasc Res. 2015;108(3):377–86.

38. Krenning G, Barauna VG, Krieger JE, Harmsen MC, Moonen JRAJ. Endothelial Plasticity: Shifting Phenotypes through Force Feedback. Vol. 2016, Stem Cells International. 2016.

39. Shimada S, Robles C, Illigens BMW, Casar Berazaluce AM, del Nido PJ, Friehs I. Distention of the Immature Left Ventricle Triggers Development of Endocardial Fibroelastosis: An Animal Model of Endocardial Fibroelastosis Introducing Morphopathological Features of Evolving Fetal Hypoplastic Left Heart Syndrome. BioMed Res Int. 2015;2015:1–10.

40. Choi SH, Hong ZY, Nam JK, Lee HJ, Jang J, Yoo RJ, et al. A hypoxia-induced vascular endothelial-to-mesenchymal transition in development of radiation-induced pulmonary fibrosis. Clin Cancer Res. 2015;21(16):3716–26.

41. Mahler GJ, Farrar EJ, Butcher JT. Inflammatory cytokines promote mesenchymal transformation in embryonic and adult valve endothelial cells. Arterioscler Thromb Vasc Biol. 2013;33(1):121–30.

42. Rabelink TJ. Endothelial Nitric Oxide Synthase: Host Defense Enzyme of the Endothelium? Arterioscler Thromb Vasc Biol. 2005 Dec 1;26(2):267–71.

43. Aisagbonhi O, Rai M, Ryzhov S, Atria N, Feoktistov I, Hatzopoulos AK. Experimental myocardial infarction triggers canonical Wnt signaling and endothelial-to-mesenchymal transition. Dis Model Mech. 2011;4(4):469–83.

44. Gasperini P, Espigol-Frigole G, McCormick PJ, Salvucci O, Maric D, Uldrick TS, et al. Kaposi sarcoma herpesvirus promotes endothelial-to-mesenchymal transition through notch-dependent signaling. Cancer Res. 2012;72(5):1157–69.

45. Gonzalez DM, Medici D. Signaling mechanisms of the epithelial-mesenchymal transition. Sci Signal. 2014;7(344):re8–re8.

46. ten Dijke P, Arthur HM. Extracellular control of TGF? signalling in vascular development and disease. Nat Rev Mol Cell Biol. 2007 Nov;8(11):857–69.

47. Oh. Inhibition of PI3 kinase/Akt pathway is required for BMP2-induced EMT and invasion. Oncol Rep [Internet]. 2009 Jul 23 [cited 2019 Oct 5];22(03). Available from: http://www.spandidos-publications.com/or/22/3/525

48. Molloy EL, Adams A, Moore JB, Masterson JC, Madrigal-Estebas L, Mahon BP, et al. BMP4 induces an epithelial–mesenchymal transition-like response in adult airway epithelial cells. Growth Factors. 2008 Jan;26(1):12–22.

49. A. van Meeteren L, Goumans M-J, ten Dijke P. TGF-β Receptor Signaling Pathways in Angiogenesis; Emerging Targets for Anti-Angiogenesis Therapy. Curr Pharm Biotechnol. 2011 Dec 1;12(12):2108–20.

50. Moustakas A. Non-Smad TGF-? signals. J Cell Sci. 2005 Aug 15;118(16):3573–84.

51. ten Dijke P, Goumans M-J, Pardali E. Endoglin in angiogenesis and vascular diseases. Angiogenesis. 2008 Mar 19;11(1):79–89.

52. Goumans M-J. Balancing the activation state of the endothelium via two distinct TGF-beta type I receptors. EMBO J. 2002 Apr 1;21(7):1743–53.

53. Goumans M-J, Valdimarsdottir G, Itoh S, Lebrin F, Larsson J, Mummery C, et al. Activin Receptor-like Kinase (ALK)1 Is an Antagonistic Mediator of Lateral TGF?/ALK5 Signaling. Mol Cell. 2003 Oct;12(4):817–28.

54. Friehs I, Illigens B, Melnychenko I, Zhong-Hu T, Zeisberg E, del Nido PJ. An animal model of endocardial fibroelastosis. J Surg Res. 2013 Jun;182(1):94–100.

55. Watabe T, Nishihara A, Mishima K, Yamashita J, Shimizu K, Miyazawa K, et al. TGF-β receptor kinase inhibitor enhances growth and integrity of embryonic stem cell–derived endothelial cells. J Cell Biol. 2003;163(6):1303–11.

56. Wu M, Peng Z, Zu C, Ma J, Lu S, Zhong J, et al. Losartan Attenuates Myocardial Endothelial-To-Mesenchymal Transition in Spontaneous Hypertensive Rats via Inhibiting TGF-β/Smad Signaling. Bader M, editor. PLOS ONE. 2016 May 13;11(5):e0155730.

57. Wu B, Zhang Z, Lui W, Chen X, Wang Y, Chamberlain AA, et al. Endocardial Cells Form the Coronary Arteries by Angiogenesis through Myocardial-Endocardial VEGF Signaling. Cell. 2012 Nov;151(5):1083–96.

58. Shiono K, Knight DW. Turbulent open-channel flows with variable depth across the channel. J Fluid Mech. 1991 Jan;222(1):617.

59. Van Meeteren LA, Ten Dijke P. Regulation of endothelial cell plasticity by TGF-β. Vol. 347, Cell and Tissue Research. 2012. p. 177–86.

60. Friehs I, Moran AM, Stamm C, Choi YH, Cowan DB, McGowan FX, et al. Promoting angiogenesis protects severely hypertrophied hearts from ischemic injury. Ann Thorac Surg. 2004;77(6):2004–10.

61. Thurston G, Baluk P, Hirata A, McDonald DM. Permeability-related changes revealed at endothelial cell borders in inflamed venules by lectin binding. Am J Physiol-Heart Circ Physiol. 1996 Dec;271(6):H2547–62.

62. Weixler V, Marx GR, Hammer PE, Emani SM, del Nido PJ, Friehs I. Flow disturbances and the development of endocardial fibroelastosis. J Thorac Cardiovasc Surg [Internet]. 2019 Sep [cited 2019 Dec 26]; Available from: https://linkinghub.elsevier.com/retrieve/pii/S0022522319319014

63. Weixler V, Hammer PE, Marx GR, Emani SM, del Nido PJ, Friehs I. Flow disturbances and progression of endocardial fibroelastosis — a case report. Cardiovasc Pathol. 2019 Sep;42:1–3.

64. Milner DJ, Taffet GE, Wang X, Pham T, Tamura T, Hartley C, et al. The absence of desmin leads to cardiomyocyte hypertrophy and cardiac dilation with compromised systolic function. J Mol Cell Cardiol. 1999 Nov;31(11):2063–76.

65. Liu S, Young SM, Varisco BM. Dynamic expression of chymotrypsin-like elastase 1 over the course of murine lung development. Am J Physiol-Lung Cell Mol Physiol. 2014 Jun;306(12):L1104–16.

66. Ren Z, Chen J, Khalil RA. Zymography as a Research Tool in the Study of Matrix Metalloproteinase Inhibitors. In: Wilkesman J, Kurz L, editors. Zymography. New York, NY: Springer New York; 2017. p. 79–102.

67. Vorisek N, Weixler H, Axt-Fliedner R, del Nido J, Friehs I. Possible Inhibitors of Endothelial-to-Mesenchymal Transition Targeting Endocardial Fibroelastosis. In Wiesbaden; 2019 [cited 2019 Dec 26]. Available from: http://www.thieme-connect.de/DOI/DOI?10.1055/s-0039-1679068

68. Kalluri R, Zeisberg M. Fibroblasts in cancer. Nat Rev Cancer. 2006 May;6(5):392–401.

69. Rieder F, Kessler SP, West GA, Bhilocha S, de la Motte C, Sadler TM, et al. Inflammation-Induced Endothelial-to-Mesenchymal Transition. Am J Pathol. 2011 Nov;179(5):2660–73.

70. Zeisberg EM, Potenta SE, Sugimoto H, Zeisberg M, Kalluri R. Fibroblasts in Kidney Fibrosis Emerge *via* Endothelial-to-Mesenchymal Transition. J Am Soc Nephrol. 2008 Dec;19(12):2282–7.

71. Suzuki M, Naruse K, Asano Y, Okamoto T, Nishikimi N, Sakurai T, et al. Up-regulation of Integrin β3Expression by Cyclic Stretch in Human Umbilical Endothelial Cells. Biochem Biophys Res Commun. 1997 Oct 20;239(2):372–6.

72. Kong P, Christia P, Saxena A, Su Y, Frangogiannis NG. Lack of specificity of fibroblast-specific protein 1 in cardiac remodeling and fibrosis. Am J Physiol Heart Circ Physiol. 2013 Nov 1;305(9):H1363-72.

73. Lopez D, Niu G, Huber P, Carter WB. Tumor-induced upregulation of Twist, Snail, and Slug represses the activity of the human VE-cadherin promoter. Arch Biochem Biophys. 2009;482(1–2):77–82.

74. Noria S, Cowan DB, Gotlieb AI, Langille BL. Transient and steady-state effects of shear stress on endothelial cell adherens junctions. Circ Res. 1999 Sep;85(6):504–14.

75. Yao Y, Jumabay M, Ly A, Radparvar M, Cubberly MR, Bostrom KI. A role for the endothelium in vascular calcification. Circ Res. 2013 Aug;113(5):495–504.

76. Woessner JFJ. Matrix metalloproteinases and their inhibitors in connective tissue remodeling. FASEB J Off Publ Fed Am Soc Exp Biol. 1991 May;5(8):2145–54.